

RESEARCH

Open Access



Prmt1-mediated methylation regulates Ncoa4 stability to transactivate *Adamts* genes and promote bone extracellular matrix degradation in chronic hematogenous osteomyelitis

Xun Chen¹, Ning Duan¹, Wentao Zhang¹, Tao Song¹ and Fei Cong^{1*}

Abstract

Background Protein arginine methyltransferases (Prmts) are essential regulators of various biological processes and have been implicated in the pathogenesis of numerous diseases. However, their role in osteomyelitis remains poorly understood.

Methods A mouse model of chronic hematogenous osteomyelitis (CHOM) was established by intravenous inoculation with *Staphylococcus aureus* (*S. aureus*). Gene and protein expression levels were quantified using RT-qPCR and immunoblot analysis, respectively. Protein interactions were determined via immunoprecipitation and co-immunoprecipitation assays. In vitro and in vivo assays were employed to evaluate protein methylation and ubiquitination. Bone destruction was assessed through histological staining.

Results Among 9 Prmt members, Prmt1 was the only one significantly upregulated in osteomyelitis-affected mice. Our findings revealed that the inflammatory microenvironment specifically upregulated Prmt1 expression in osteoblasts and osteocytes, which facilitated its interaction with the transcriptional activator Ncoa4 (nuclear receptor coactivator 4) and mediated Ncoa4 arginine methylation, thereby enhancing Ncoa4 protein stability. Methylated Ncoa4 formed a transcriptional complex with the histone acetyltransferase Cbp (CREB-binding protein) and transcription factor Ap1 (Activator protein 1), driving the expression of four *Adamts* genes (*Adamts3/8/12/14*) that promoted extracellular matrix (ECM) degradation in osteoblasts and osteocytes. In contrast, depletion or pharmacological inhibition of Prmt1 prevented Ncoa4 methylation upon stimulation with pro-inflammatory cytokines, leading to Ncoa4 ubiquitination by Rnf8 (Ring finger protein 8) E3 ligase and subsequent proteasomal degradation, eventually leading to downregulation of *Adamts* expression. Importantly, treatment with Prmt1 inhibitors TCE-5003 and MS023 significantly mitigated bone ECM degradation and prevented osteomyelitis progression in *S. aureus*-infected mice.

*Correspondence:

Fei Cong
fei.cong21@outlook.com

Full list of author information is available at the end of the article



© The Author(s) 2025. **Open Access** This article is licensed under a Creative Commons Attribution-NonCommercial-NoDerivatives 4.0 International License, which permits any non-commercial use, sharing, distribution and reproduction in any medium or format, as long as you give appropriate credit to the original author(s) and the source, provide a link to the Creative Commons licence, and indicate if you modified the licensed material. You do not have permission under this licence to share adapted material derived from this article or parts of it. The images or other third party material in this article are included in the article's Creative Commons licence, unless indicated otherwise in a credit line to the material. If material is not included in the article's Creative Commons licence and your intended use is not permitted by statutory regulation or exceeds the permitted use, you will need to obtain permission directly from the copyright holder. To view a copy of this licence, visit <http://creativecommons.org/licenses/by-nc-nd/4.0/>.

Conclusion These findings identify Prmt1 as a pivotal regulator of bone ECM degradation in osteomyelitis through stabilization of Ncoa4 and highlight Prmt1 as a promising therapeutic target for osteomyelitis treatment.

Keywords Osteomyelitis, Prmt1, Ncoa4, Ap1, Adamts, Rnf8, ECM degradation

Introduction

Osteomyelitis is a severe bone infection characterized by inflammation and tissue destruction, typically caused by bacterial pathogens, with *Staphylococcus aureus* (*S. aureus*) being the most common causative agent [1, 2]. This condition can arise either from hematogenous spread, where bacteria enter the bloodstream and localize in the bone, or from contiguous spread, such as direct inoculation through trauma or surgical procedures [1, 2, 5]. Osteomyelitis can be classified into acute and chronic forms based on clinical and histopathological findings [1, 2]. Acute osteomyelitis develops rapidly, typically within two weeks, and is associated with intense inflammation without necrotic bone formation [1, 2]. In contrast, chronic hematogenous osteomyelitis (CHOM) evolves over weeks to months, often resulting in necrotic bone tissue and sequestra, complicating both the infection and its treatment [3, 4].

CHOM arises from intricate interactions among the host immune system, bacterial virulence factors, and dysregulated inflammatory responses [3, 4]. A central molecular mechanism in CHOM pathogenesis is the ability of *S. aureus* (the most common causative pathogen) to evade host immune defenses [3, 4]. This pathogen achieves immune evasion by forming biofilms, secreting virulence factors such as alpha-toxin, and invading both phagocytic and non-phagocytic cells, including osteoblasts and macrophages [3, 4]. Within macrophages, *S. aureus* survives intracellularly by suppressing mitochondrial reactive oxygen species (mtROS) production, which impairs the bactericidal activity of these immune cells [5]. Furthermore, *S. aureus* drives excessive activation of inflammatory pathways such as nuclear factor-kappa B (NF- κ B) and mitogen-activated protein kinases (MAPKs) [6, 7], resulting in the release of pro-inflammatory cytokines [e.g., tumor necrosis factor-alpha (TNF- α) and interleukin-1 beta (IL-1 β)] and the over-recruitment of neutrophils [6, 7]. This persistent inflammatory state promotes bone destruction through the upregulation of matrix-degrading enzymes like matrix metalloproteinases (Mmps) and a disintegrin and metalloproteinase with thrombospondin motifs (Adamts), as well as receptor activator of nuclear factor- κ B ligand (Rankl)-mediated osteoclast activation, which accelerates bone resorption [8–10]. The breakdown of the bone extracellular matrix (ECM) by Mmps and Adamts undermines the structural integrity of the bone [11, 12]. The ECM itself consists of organic components, inorganic minerals, cellular elements, and water, with the periosteum, cortical

bone, trabecular bone, and endosteum contributing to its overall architecture and function [13, 14]. The bone marrow also plays a vital role in repair and regeneration [13, 14]. Additionally, the formation of necrotic bone (sequestra) during CHOM further complicates treatment by shielding bacteria from immune clearance and limiting antibiotic efficacy [15].

Protein arginine methyltransferases (Prmts) are a family of enzymes that mediate the methylation of arginine residues in proteins, a key post-translational modification that influences a wide range of cellular processes [16, 17]. The Prmt family consists of nine members in mammals, categorized into three types based on the type of methylation they catalyze [16, 17]. Type I Prmts (Prmt1, Prmt2, Prmt3, Prmt4/Carm1, Prmt6, and Prmt8) catalyze asymmetric dimethylation of arginine, type II Prmts (Prmt5 and Prmt9) mediate symmetric dimethylation, while type III PRMT (Prmt7) generates monomethylarginine exclusively [16, 17]. Each Prmt member has distinct yet overlapping roles in regulating cellular physiology. Prmt1, the most abundant and well-studied member of the family, is responsible for the majority of asymmetric dimethylarginine modifications in cells [16, 17]. Prmt1 regulates transcription by methylating histones, such as H4R3, to promote chromatin remodeling and gene activation. It also stabilizes key proteins by methylating their arginine residues, thus influencing their stability, localization, or interaction with binding partners [16, 17]. For instance, Prmt1-mediated methylation of p53 enhances its tumor-suppressive functions [18], while methylation of Foxo1 (Forkhead box O1) transcription factors modulates metabolic pathways [19]. The dysregulation of Prmts has been implicated in numerous diseases. Prmt1 and Prmt5 are frequently overexpressed in cancers, where they drive tumorigenesis by modulating oncogenic pathways and immune evasion [20]. Prmt4 has been linked to autoimmune diseases through its role in T cell differentiation [21], and Prmt7 is associated with cellular stress responses and metabolic disorders [22]. Despite these well-established roles, the involvement of Prmt family members in osteomyelitis remains poorly understood.

To investigate the role of Prmt family members in the pathogenesis of *S. aureus*-induced CHOM, we established a CHOM mouse model. Analysis of Prmt expression in the tibiae of infected mice revealed that only Prmt1 was significantly upregulated, while other members showed no notable changes. Our in vivo and in vitro studies demonstrated that Prmt1 was upregulated in an inflammatory microenvironment, where it

methylated and stabilized the transcriptional activator Ncoa4 (nuclear receptor coactivator 4). Stabilized Ncoa4 forms a complex with the histone acetyltransferase Cbp (CREB-binding protein) and the transcription factor Ap1 (Activator protein 1), which binds to the promoter regions of four *Adamts* genes (*Adamts3/8/12/14*) to activate their expression. These matrix-degrading enzymes were secreted from osteoblasts and osteocytes, promoting bone ECM degradation and exacerbating bone destruction. Furthermore, Prmt1 inhibitors effectively destabilized Ncoa4 by inducing its Rnf8 (Ring finger protein 8)-dependent ubiquitination and proteasomal degradation, leading to suppressed *Adamts* expression. These findings highlight the critical role of Prmt1-Ncoa4-Cbp-Ap1 axis signaling in promoting bone ECM degradation in CHOM.

Materials and methods

Culture of *S. aureus*

To culture *S. aureus* strain 6850, obtained from the American Type Culture Collection (ATCC) (Manassas, VA, USA; #53657), the strain was initially recovered on solid brain heart infusion (BHI) broth (Sigma-Aldrich, Shanghai, China; #53286) at 37 °C for 20 h. A single bacterial colony was then selected and cultured in 30 mL of liquid BHI medium at 37 °C with shaking at 200 rpm for 18 h to reach the mid-log phase. The culture was adjusted to an OD₆₀₀ of 1.0 to ensure the appropriate bacterial concentration. The inoculum was prepared by centrifuging the bacteria and diluting with phosphate-buffered saline (PBS) (Thermo Fisher, Shanghai, China; #10010023). All procedures were carried out under sterile conditions to prevent contamination and ensure the integrity of the bacterial culture.

Animal experiments

All animal experiments were conducted in accordance with a protocol (XAH-22-012) approved by the Institutional Animal Care and Use Committee of Honghui Hospital. C57BL/6 mice were obtained from Beijing Vital River Laboratory Animal Technology Co., Ltd., and housed under standard conditions with a 12-hour light/dark cycle. Eight-week-old C57BL/6 mice (22–25 g) were anesthetized using 3% isoflurane (Sigma-Aldrich; #792632) and randomly divided into experimental groups. In one experiment, mice were assigned to two groups ($n=8$ per group): one group received 100 μ L PBS via tail vein injection, while the other group was injected with a bacterial suspension (1×10^8 CFU/mL) to induce osteomyelitis. In another experiment designed to evaluate the effects of Prmt1 inhibitors on CHOM, mice were divided into four groups ($n=8$ per group): Group 1 received 100 μ L PBS as a control; Group 2 was injected with a 100 μ L suspension of *S. aureus* (1×10^8 CFU/

mL); Group 3 received *S. aureus* followed by intraperitoneal injections of TCE-5003 (50 mg/kg, a Prmt1 inhibitor; Selleckchem, #S0855) every five days for 6 weeks; Group 4 received *S. aureus* followed by intraperitoneal injections of MS023 (50 mg/kg, a Type I Prmt inhibitor; Selleckchem, #S8112) every five days for 6 weeks. Throughout the study, mice were monitored daily for infection signs, and body weight was recorded bi-weekly. At 6 weeks post-inoculation, all mice were euthanized, and infected bones were collected for histopathological analysis, micro-CT imaging, and molecular assessments.

Cell culture and transfection

In this study, we employed several mouse cell lines representing distinct bone cell types. Specifically, the osteoblast cell line MC3T3-E1 (Sigma-Aldrich, #99072810) and the osteocyte cell line MOCY-1 (Creative Bioarray, Shirley, NY, USA; #CSC-C5334S) were used. Additionally, the osteoclast cell line MOCPC-5 (Cellosaurus, Swiss Institute of Bioinformatics; #CVCL_F699) and the bone marrow macrophage cell line MBMM-1 (Creative Bioarray; #CSC-C1940) were included. All cells were cultured in Dulbecco's Modified Eagle Medium (DMEM) (Thermo Fisher; #11965092), supplemented with 10% (v/v) fetal bovine serum (FBS) (Thermo Fisher; #A5670701) and 1% penicillin/streptomycin (Thermo Fisher; #15140122). Cultures were maintained in a humidified incubator at 37 °C with 5% CO₂. When cells reached 80% confluence, they were harvested using 0.25% trypsin-EDTA (Thermo Fisher; #25200072) and resuspended in Opti-MEM™ I Reduced Serum Medium (Thermo Fisher; #31985070) for subsequent experiments. Transfections were performed using Lipofectamine transfection reagent (Thermo Fisher; #18324012) with short hairpin RNAs (shRNAs) and plasmids, as detailed in Tables S1 and S2, following the manufacturer's instructions.

Enzyme-Linked Immunosorbent Assay (ELISA)

Mouse blood samples were collected and allowed to clot at room temperature for 30 min. This was followed by centrifugation at $2,000 \times g$ for 20 min to separate the serum. The serum samples were then used to determine the circulating concentrations of IL-1 β , IL-6, and TNF- α using their respective ELISA kits (IL-1 β ELISA kit: Thermo Fisher, #BMS6002; IL-6 ELISA kit: Thermo Fisher, #KMC0061; TNF- α ELISA kit: Thermo Fisher, #BMS607HS).

Cell treatments

Cells at 80% confluence were treated with various concentrations (0, 10, 20, and 40 ng/mL) of IL-1 β (Sigma-Aldrich; #I5271) and TNF- α (Sigma-Aldrich; #T7539) for 6 h, followed by two washes with cold PBS. Additionally, Cells at 80% confluence were co-treated with 40 ng/mL

IL-1 β and different concentrations of TCE-5003 (0, 3, and 6 μ M) or with 40 ng/mL IL-1 β and different concentrations of MS023 (0, 100, and 200 nM) for 6 h, followed by two washes with cold PBS. The resulting cells were used for RNA and protein isolation.

RNA isolation and real-time quantitative polymerase chain reaction (RT-qPCR)

RNA was extracted from cultured cells and mouse tibiae using TRIzol Reagent (Sigma-Aldrich; #T9424) according to the manufacturer's protocol. For cell samples, cells were washed with PBS and lysed directly in TRIzol. For tissue samples, infected tibiae were ground into a fine powder under liquid nitrogen prior to homogenization in TRIzol. The extracted RNA was quantified, and reverse transcription into cDNA was performed using the High-Capacity cDNA Reverse Transcription Kit (Thermo Fisher; #4368814). Gene expression analysis was conducted via RT-qPCR using PowerUp SYBR Green Master Mix (Thermo Fisher; #A25742) on an Applied Biosystems QuantStudio 3 system. Beta-Actin served as the internal reference gene, and relative gene expression levels were calculated using the $2^{-\Delta\Delta C_t}$ method. Primer sequences used for qPCR are listed in Table S3.

Protein isolation and immunoblots

Cells were first washed with cold PBS and lysed using radio-immunoprecipitation assay (RIPA) buffer (Sigma-Aldrich; #R0278) supplemented with protease and phosphatase inhibitors (Sigma-Aldrich; # P8340). Infected bone tissues were homogenized in liquid nitrogen and then lysed with RIPA buffer containing the same inhibitors. Lysates were centrifuged at 12,000 g for 15 min at 4 $^{\circ}$ C, and the supernatant was collected. Protein concentration was determined using the BCA Protein Assay Kit (Sigma-Aldrich; #71285). Equal amounts of protein (50 μ g) were separated by SDS-PAGE and transferred onto polyvinylidene difluoride (PVDF) membranes (Sigma-Aldrich; # IPVH09120). Membranes were blocked with 5% non-fat dry milk (Cell signaling, Shanghai, China; #9999S) in TBS-T for 1 h at room temperature and incubated overnight at 4 $^{\circ}$ C with primary antibodies (Table S4). After washing, membranes were incubated with HRP-conjugated secondary antibodies (Table S4) for 1 h at room temperature. Protein bands were visualized using the ECL (enhanced chemiluminescence) Western Blotting Detection Reagent (Thermo Fisher; #32109). Band intensities were quantified using ImageJ software and normalized to GAPDH.

Isobaric tags for relative and absolute quantitation (iTRAQ)

The iTRAQ assay was performed following an established protocol [23]. Briefly, cell lysates were prepared with a lysis buffer containing 8 M urea, 75 mM NaCl, 50

mM Tris-HCl (pH 8.2), 1 mM EDTA, 2 μ g/mL aprotinin, 2 μ g/mL leupeptin, 1 mM PMSF, and 1 mM Na₃VO₄. The lysates were sonicated on ice, centrifuged, and protein concentrations determined using the BCA Protein Assay Kit. Proteins were reduced, alkylated, and digested with trypsin (Thermo Fisher; #90057). Peptides were labeled with iTRAQ reagents (Sigma-Aldrich; #4381663-1KT), pooled, and dried by vacuum centrifugation. Fractionation was done by strong cation exchange chromatography and desalted. Peptides were analyzed by liquid chromatography with tandem mass spectrometry (LC-MS/MS). Data were processed using Proteome Discoverer software (Thermo Fisher; #B51001473), with protein identification and relative quantitation performed based on reporter ion intensities, using a UniProt mouse database with a false discovery rate (FDR) of less than 1%.

Immunoprecipitation (IP) and mass spectrometry (MS) analysis

Infected tibiae tissues were homogenized in IP lysis buffer containing 50 mM Tris-HCl (pH 7.4), 150 mM NaCl, 1 mM EDTA, 1% NP-40, 0.5% sodium deoxycholate, and protease/phosphatase inhibitor cocktails. Homogenates were centrifuged at 13,000 g for 15 min to remove debris, and the supernatants were pre-cleared with Protein A/G agarose beads (Thermo Fisher; #20421). Pre-cleared lysates were incubated with anti-Prmt1 antibody, anti-Ncoa4 (Table S4), or control IgG (Thermo Fisher; #10400 C) overnight at 4 $^{\circ}$ C with gentle rotation. Immunocomplexes were captured using Protein A/G agarose beads, washed extensively with lysis buffer, and eluted. Eluted proteins were separated by SDS-PAGE, stained, and bands of interest were excised and subjected to in-gel tryptic digestion. The resulting peptides were analyzed by LC-MS/MS. Data were processed using Proteome Discoverer software, and protein identification was performed with an FDR of less than 1%, using a UniProt mouse database.

Co-immunoprecipitation (Co-IP) assay

The coding sequences of *Prmt1*, *Ncoa4*, *Cbp*, *c-Jun*, and *c-Fos* were amplified from mouse tibial cDNA and cloned into pCDNA3.1-Flag and pCDNA3.1-HA expression vectors. Primer sequences and restriction enzyme sites used for cloning were listed in Table S2. All constructs were verified by sequencing to ensure sequence accuracy. Cells at 80% confluence were co-transfected with HA-tagged and Flag-tagged vectors using Lipofectamine transfection reagent. After 48 h, cells were lysed in RIPA lysis buffer supplemented with protease and phosphatase inhibitors. Lysates were clarified by centrifugation at 13,000 g for 15 min and the supernatants was incubated with anti-Flag magnetic agarose beads (Thermo Fisher; #A36797) overnight at 4 $^{\circ}$ C. Beads were washed and bound proteins

were eluted by boiling in SDS sample buffer. Eluted proteins were resolved by SDS-PAGE, transferred to PVDF membranes, and blocked with non-fat dry milk. Membranes were incubated with primary antibodies against Myc and Flag, followed by HRP-conjugated secondary antibodies (Table S4). Protein bands were visualized using an ECL detection system.

Chromatin Immunoprecipitation (ChIP) assay

Cells were cultured to 80% confluence then crosslinked with 1% formaldehyde (Sigma-Aldrich; #252549) for 10 min at room temperature to preserve protein-DNA interactions, followed by quenching with 125 mM glycine for 5 min. Cells were harvested and lysed in ChIP lysis buffer [50 mM Tris-HCl (pH 8.0), 10 mM EDTA, 1% SDS, 150 mM NaCl, and 1% Triton X-100] containing protease inhibitors. The chromatin was sheared to an average length of 200–500 bp by sonication. The lysates were cleared by centrifugation at 13,000 *g* for 15 min and the supernatant was incubated with anti-Ncoa4, anti-Cbp, anti-c-Jun, anti-c-Fos, or IgG control (Table S4) overnight at 4 °C. Protein G agarose beads (Thermo Fisher; #20397) were added and incubated for an additional 2 h at 4 °C. Beads were washed five times with lysis buffer. The protein-DNA complexes were eluted from the beads with elution buffer and reverse crosslinked by heating at 65 °C for 4 h. DNA was purified using a PCR purification kit (ZYMO Research, Shanghai, China; #D5205) and quantified by RT-qPCR with specific primers (Table S5) to detect the binding of Ncoa4, Cbp, c-Jun, and c-Fos to the promoter regions of target genes.

Hematoxylin and Eosin (H&E) staining

Mouse tibiae were collected and fixed in 10% neutral buffered formalin (Sigma-Aldrich; #HT501128) for 24 h at room temperature. Following fixation, the samples were decalcified in 10% EDTA (pH 7.4) for 4 weeks, with the solution changed every 2–3 days until the bones were sufficiently pliable. Decalcified samples were processed through a series of ethanol washes, including 70% ethanol, 95% ethanol, and 100% ethanol for 2 min each, cleared in xylene, and embedded in paraffin, cleared in xylene, and embedded in paraffin. Paraffin-embedded bone samples were sectioned at 5 µm thickness using a rotary microtome and mounted on positively charged glass slides. The sections were deparaffinized in xylene (three changes, 5 min each), rehydrated through graded ethanol (100%, 95%, 70%, and 50% for 2 min each), and then rinsed in distilled water. For Hematoxylin staining, the sections were immersed in Harris hematoxylin solution for 5 min, followed by rinsing in running tap water for 5 min to remove excess stain. Differentiation was carried out using 1% acid alcohol (1% hydrochloric acid in 70% ethanol) for a few seconds, and sections were

subsequently blued in 0.2% ammonia water for 1 min. The sections were then washed in running tap water for 5 min, followed by staining with an H&E kit (Abcam, Shanghai, China; #ab245880). Stained sections were examined under a light microscope, and digital images were captured using a Leica DM2000 microscope.

Protein purification and in vitro methylation detection

To express and purify His-tagged Ncoa4 and GST-tagged Prmt1, plasmids encoding His-Ncoa4 and GST-Prmt1 (Table S2) were transformed into *E. coli* BL21 (DE3) competent cells. Cultures were grown in Luria-Bertani broth (LB) medium containing 100 µg/mL ampicillin (Sigma-Aldrich; #A9518) for His-Ncoa4 or 50 µg/mL kanamycin (Sigma-Aldrich; #K1377) for GST-Prmt1 at 37 °C until the OD₆₀₀ reached 0.6–0.8. Protein expression was induced by adding 0.5 mM Isopropyl β-D-1-thiogalactopyranoside (IPTG) (Sigma-Aldrich; #I6758), and cultures were incubated at 16 °C overnight. For His-Ncoa4 purification, cells were resuspended in lysis buffer (50 mM Tris-HCl pH 8.0, 300 mM NaCl, 10 mM imidazole, 1 mM PMSE, and 0.1% Triton X-100) and lysed by ultrasonication. The lysates were centrifuged at 12,000 × *g* for 20 min at 4 °C, and the supernatant was incubated with Ni-NTA resin (Qiagen, Shanghai, China; #30210). Proteins were eluted with buffer containing 50 mM Tris-HCl pH 8.0, 300 mM NaCl, and 250 mM imidazole. For GST-Prmt1 purification, cells were lysed in buffer (50 mM Tris-HCl pH 8.0, 150 mM NaCl, 1 mM PMSE, and 1% Triton X-100) and processed similarly. Lysates were incubated with GST-Sepharose beads (Sigma-Aldrich; #GE17-0756-05), and GST-tagged proteins were eluted with buffer containing 50 mM Tris-HCl pH 8.0, 150 mM NaCl, and 10 mM reduced glutathione. For the in vitro methylation assay, reaction mixtures (30 µL) contained 50 mM Tris-HCl pH 8.0, 50 mM NaCl, 1 mM DTT, 0.5 µg His-Ncoa4, 0.5 µg GST-Prmt1, and 1 µM S-adenosylmethionine (SAM, Sigma-Aldrich; #A7007). Reactions were incubated at 30 °C for 1 h and terminated by adding SDS-PAGE loading buffer. Proteins were resolved by SDS-PAGE, transferred to PVDF membranes, and probed with an anti-ADMA antibody (Table S4).

In vitro and in vivo ubiquitination assays

For in vitro ubiquitination assay, His-tagged Ncoa4 was purified from *E. coli* and incubated in a reaction mixture containing commercially available E1 (Uae1, Sigma-Aldrich; #U5633), E2 (UbcH5c, Sigma-Aldrich; #23-035-M), GST-tagged Rnf8, 2 mM ATP, and ubiquitin (Sigma-Aldrich; #U5507) in ubiquitination buffer (50 mM Tris-HCl pH 7.5, 50 mM NaCl, 5 mM MgCl₂, and 1 mM DTT). The reaction was performed at 30 °C for 1 h. Ubiquitination of Ncoa4 was analyzed by SDS-PAGE followed by Western blotting using an anti-ubiquitin

antibody (Table S4). Negative controls, omitting Rnf8, E1, or E2, were included to confirm the specificity of the ubiquitination reaction.

For in vivo ubiquitination assay, MC3T3-E1 cells were transfected with plasmids encoding Flag-Ncoa4, HA-ubiquitin, and Myc-Rnf8 (Table S2) using Lipofectamine transfection reagent. After 48 h of transfection, cells were treated with 40 ng/mL IL-1 β for 6 h. Cells were lysed in RIPA buffer supplemented with protease inhibitors and 10 μ M MG132 (Thermo Fisher; #J63250.MCR) to inhibit proteasomal degradation of ubiquitinated proteins. Lysates were cleared by centrifugation, and Flag-Ncoa4 was immunoprecipitated using anti-Flag magnetic Agarose. Immunoprecipitates were analyzed by Western blotting using an anti-HA antibody (Table S4).

Statistical analysis

All experiments in this study were independently repeated in triplicate. Data were expressed as mean \pm standard deviation (SD) from at least three independent experiments. Statistical comparisons between two groups were performed using an unpaired Student's *t*-test. For comparisons involving more than two groups, one-way analysis of variance (ANOVA) followed by Tukey's post hoc test was employed to determine the statistical significance. GraphPad Prism 8.0 software (GraphPad Software, La Jolla, CA, USA) was used for all statistical analyses. A *P*-value of less than 0.05 was considered statistically significant. Statistical significance levels were denoted as follows: **P* < 0.05, ***P* < 0.01, and ****P* < 0.001.

Results

Prmt1 was upregulated in CHOM mice

To explore the potential roles of Prmts in the pathology of CHOM, we established both control and CHOM mouse models. This was achieved by administering tail vein injections of PBS and *S. aureus*, respectively, to C57BL/6J mice (Fig. 1A). Six weeks post-injection, ELISA analysis of serum pro-inflammatory cytokines revealed significant increases in IL-1 β , IL-6, and TNF- α levels in the CHOM group compared to controls (Fig. 1B and D). Inflammatory lesions in the tibiae were markedly more pronounced in CHOM mice than in controls (Fig. 1E), and H&E staining further demonstrated a greater extent of bone destruction in CHOM mice (Fig. 1F). Additionally, colony-forming unit (CFU) assays of tibia homogenates showed a significantly higher bacterial load of *S. aureus* in CHOM mice compared to controls (Fig. 1G).

Following the successful validation of the CHOM model, we proceeded to evaluate the mRNA and protein expression profiles of Prmt1-9 in the tibiae of both groups. Our findings revealed that Prmt1 was uniquely upregulated at both transcriptional and translational

levels in CHOM mice, while the expression patterns of the remaining eight Prmts showed no significant inter-group differences (Fig. 1H and Q). These results suggest a potential specific involvement of Prmt1 in the pathogenesis of CHOM.

Prmt1 was upregulated in IL-1 β - or TNF- α -treated osteoblast and osteocyte cells

To investigate whether the upregulation of Prmt1 observed in CHOM mice is attributed to the inflammatory microenvironment, we treated various bone-related cell lines with IL-1 β and TNF- α at different concentrations (0, 10, 20, and 40 ng/mL). The cell lines included an osteoblast line (MC3T3-E1), an osteocyte line (MOCY-1), an osteoclast line (MOCP-5), and a bone marrow macrophage line (MBMM-1). Following treatment, the expression levels of Prmt1-9 were assessed. Consistent with the findings in CHOM mice, Prmt1 expression was significantly upregulated in IL-1 β - and TNF- α -treated MC3T3-E1 and MOCY-1 cells, while the other eight *Prmt* genes showed no significant changes (Figures S1 and S2). Interestingly, none of the *Prmts*, including *Prmt1*, displayed notable changes in expression levels in MOCP-5 and MBMM-1 cells upon IL-1 β and TNF- α treatment (Figure S3). These results suggest that the inflammatory microenvironment specifically regulates Prmt1 expression in osteoblast and osteocyte cells but not in osteoclasts or bone marrow macrophages, highlighting a cell type-dependent response to inflammatory stimuli. Given the consistent expression of Prmt1 in osteoblast and osteocyte cells following IL-1 β or TNF- α treatment, we will primarily use the MC3T3-E1 osteoblast cell line and IL-1 β stimulation for subsequent cellular studies, unless otherwise specified.

Ncoa4 and Adamts3/8/12/14 were dependent on Prmt1

To elucidate the role of Prmt1 in the pathogenesis of osteomyelitis, we next sought to identify its downstream targets. To this end, we generated a Prmt1 knockdown cell line (Prmt1^{KD}) in MC3T3-E1 cells (Figures S4A and S4B). Control^{KD} and Prmt1^{KD} cells were treated with either PBS (control) or 40 ng/mL IL-1 β , followed by iTRAQ-based proteomic analysis (Fig. 2A). In Control^{KD} cells, IL-1 β treatment resulted in 811 differentially expressed proteins compared to PBS-treated controls, with 435 upregulated and 376 downregulated (Fig. 2B). Similarly, in Prmt1^{KD} cells, IL-1 β treatment induced differential expression of 936 proteins relative to PBS-treated Prmt1^{KD} cells, with 479 upregulated and 459 downregulated (Fig. 2C). Comparative analysis of the iTRAQ data across the four groups revealed that IL-1 β treatment in Control^{KD} cells led to the upregulation of Ncoa4 and Adamts3/8/12/14. In contrast, these proteins remained unchanged in Prmt1^{KD} cells compared

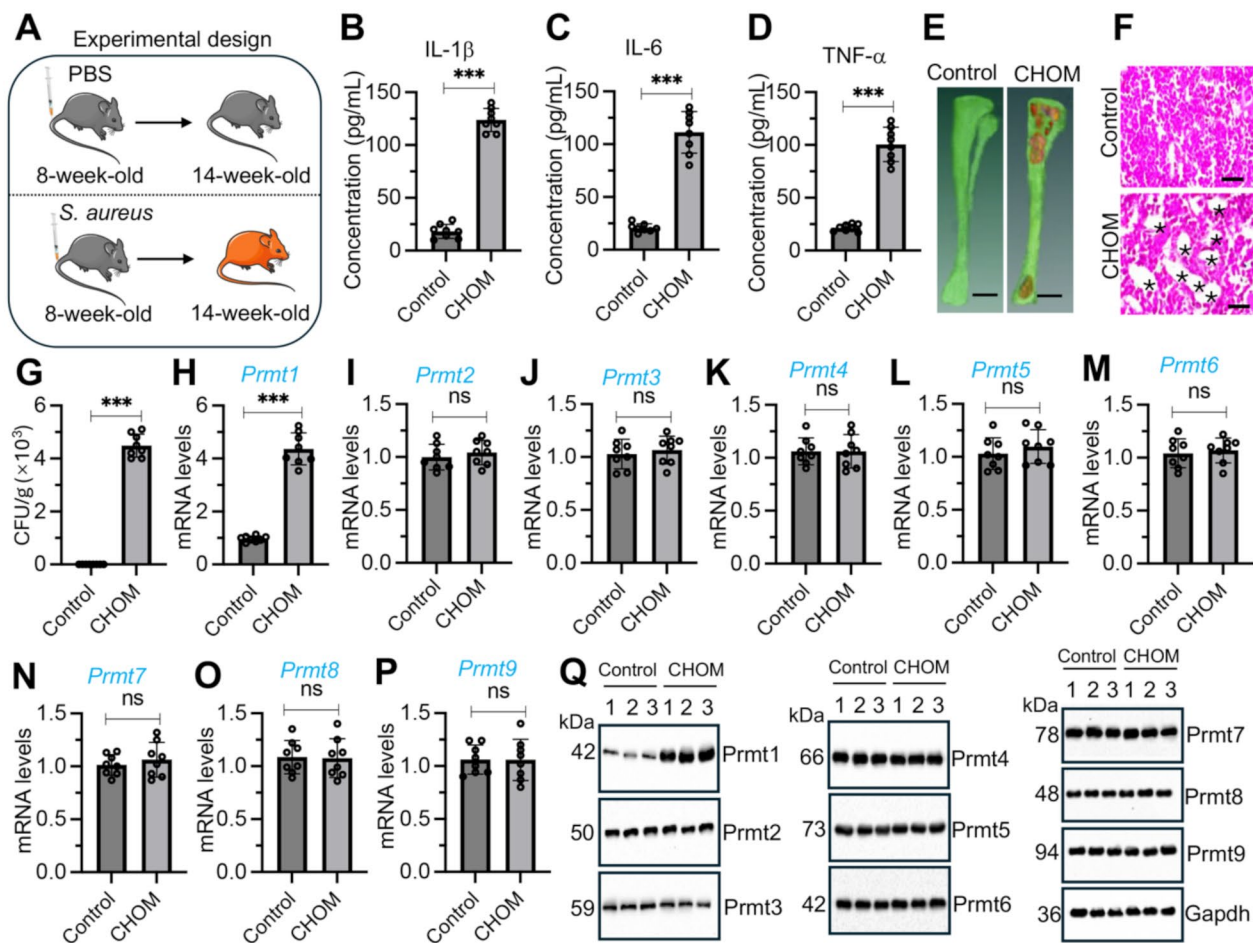


Fig. 1 Prmt1 were upregulated in CHOM mice. **(A)** Schematic models of CHOM mice. **(B-D)** Serum concentrations of IL-1 β **(B)**, IL-6 **(C)**, and TNF- α **(D)** in Control and CHOM mice ($n=8$ per group). **(E)** Representative images of inflammatory lesions in tibiae from Control and CHOM mice. **(F)** Representative images of H&E staining in tibiae from Control and CHOM mice. Asterisks (*) indicated areas of sequestrum formation. **(G)** Bacterial CFU numbers in Control and CHOM mice. Homogenates prepared from 1 g of tibiae from each group of mice were plated onto Tryptic Soy Agar (TSA) plates. The plates were incubated at 37 $^{\circ}$ C for 20 h, and the resulting colonies were counted. **(H-P)** mRNA levels of *Prmt1-9* in Control and CHOM mice ($n=8$ per group). **(H)***Prmt1*; **(I)***Prmt2*; **(J)***Prmt3*; **(K)***Prmt4*; **(L)***Prmt5*; **(M)***Prmt6*; **(N)***Prmt7*; **(O)***Prmt8*; **(P)***Prmt9*. **(Q)** Protein levels of Prmt1-9 in the tibiae tissues from Control and CHOM mice ($n=3$ per group). ns: no significant difference; ** $P<0.01$; *** $P<0.001$

to Control^{KD} cells, and their expression was significantly downregulated in IL-1 β -treated Prmt1^{KD} cells (Fig. 2D and Table S6). We also detected protein levels of Prmt1, Ncoa4, Adamts3/8/12/14, Hrnkp (Heterogeneous nuclear ribonucleoprotein K), Habp4 (Hyaluronan-binding protein 4), Grwd1 (Glutamate-rich WD repeat-containing protein 1), Btg2 (BTG family member 2), Ctu1 (Cytoplasmic tRNA 2-thiolation protein 1), G3bp2 (Ras GTPase-activating protein-binding protein 2), and Cyth2 (Cytohesin-2) in Control^{KD} and Prmt1^{KD} cells treated with or without IL-1 β . Among the proteins analyzed, the expression levels of Ncoa4 and Adamts3/8/12/14 were significantly upregulated in IL-1 β -treated Control^{KD} cells. In Prmt1^{KD} cells without IL-1 β treatment, the expression of these proteins did not differ significantly from that in untreated Control^{KD} cells (Fig. 2E and

F). However, IL-1 β treatment of Prmt1^{KD} cells led to a marked decrease in Ncoa4 and Adamts3/8/12/14 levels compared to their untreated counterparts (Fig. 2E and F). Similarly, in IL-1 β -treated Control^{KD} cells, the expression of Habp4, Grwd1, Btg2, Ctu1, G3bp2, and Cythd was significantly reduced relative to untreated Control^{KD} cells (Fig. 2F). In Prmt1^{KD} cells without IL-1 β treatment, the levels of these proteins were comparable to those in IL-1 β -treated Control^{KD} cells (Fig. 2F). In contrast, when Prmt1^{KD} cells were exposed to IL-1 β , the expression of Habp4, Grwd1, Btg2, Ctu1, G3bp2, and Cythd was significantly elevated compared to untreated Prmt1^{KD} cells (Fig. 2F). We also generated Control^{KD} and Prmt1^{KD} cells using the MOCY-1 osteocyte cell line (Figures S4C and S4D) and treated them with or without 40 ng/mL IL-1 β . The protein expression profiles obtained in this system

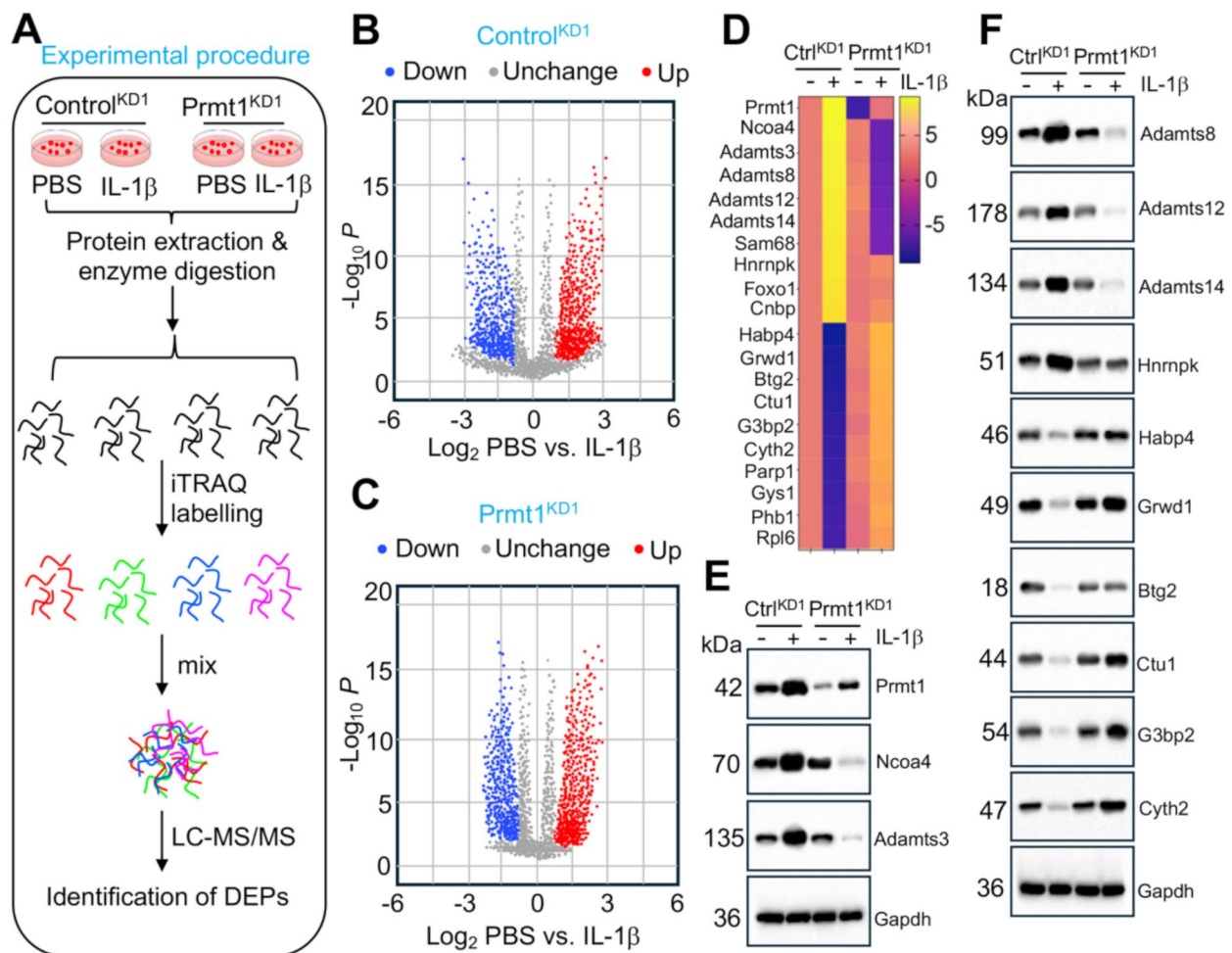


Fig. 2 Expression of Ncoa4 and Adamts3/8/12/14 was dependent on Prmt1 in MC3T3-E1 cells. **(A)** Schematic of iTRAQ analysis in Control^{KD} and Prmt1^{KD} cells (MC3T3-E1 background) treated with PBS or 40 ng/mL IL-1 β for 6 h. **(B and C)** Volcano plots illustrating the \log_2 fold changes. Red dots represent upregulated proteins; grey dots represent unchanged proteins; blue dots represent downregulated proteins. **(B)** PBS vs. IL-1 β in Control^{KD} cells. **(C)** PBS vs. IL-1 β in Prmt1^{KD} cells. **(D)** Heatmap showing the top 20 most significantly dysregulated proteins. **(E and F)** Validation of protein expression levels for Prmt1, Ncoa4, Adamts3/8/12/14, Hnrnpk, Habp4, Grwd1, Btg2, Ctu1, G3bp2, and Cyth2 in Control^{KD} and Prmt1^{KD} cells treated with PBS and 40 ng/mL IL-1 β for 6 h

were entirely consistent with those observed in IL-1 β -treated Control^{KD} and Prmt1^{KD} cells derived from the MC3T3-E1 background (Figures S5A and S5B).

We also treated MC3T3-E1 cells with TCE-5003 (0, 3, and 6 μ M) or MS023 (0, 100, and 200 nM) in combination with 40 ng/mL IL-1 β . The results demonstrated that in both cell lines, treatment with TCE-5003 or MS023 led to a dose-dependent reduction in the protein levels of Ncoa4 and Adamts3/8/12/14 (Figures S5C and S5D). These results suggest that the expression of Ncoa4 and Adamts3/8/12/14 is dependent on Prmt1. Notably, Prmt1 depletion or inhibition led to the downregulation of Ncoa4 and Adamts3/8/12/14 specifically under IL-1 β stimulation, underscoring the critical role of Prmt1 in mediating the inflammatory response in osteoblast and osteocytes.

Prmt1 directly interacted with and methylated Ncoa4 to promote transcriptional complex assembly with Cbp and Ap1

Given the observed upregulation of Prmt1 in CHOM mice, we evaluated the global arginine methylation levels in total tissue lysates from CHOM-tibiae using an anti-ADMA antibody. The results revealed significantly higher methylation signal intensities in CHOM-tibiae compared to control mice (Fig. 3A). To identify potential Prmt1 target proteins, we performed IP experiments in CHOM-tibiae tissues using IgG and anti-Prmt1-conjugated agarose beads. Mass spectrometry analysis of the purified proteins identified Ncoa4, Cbp, and Ap1 subunits (c-Jun and c-Fos) as candidates (Table S7). Independent validation experiments in the same CHOM-tibiae

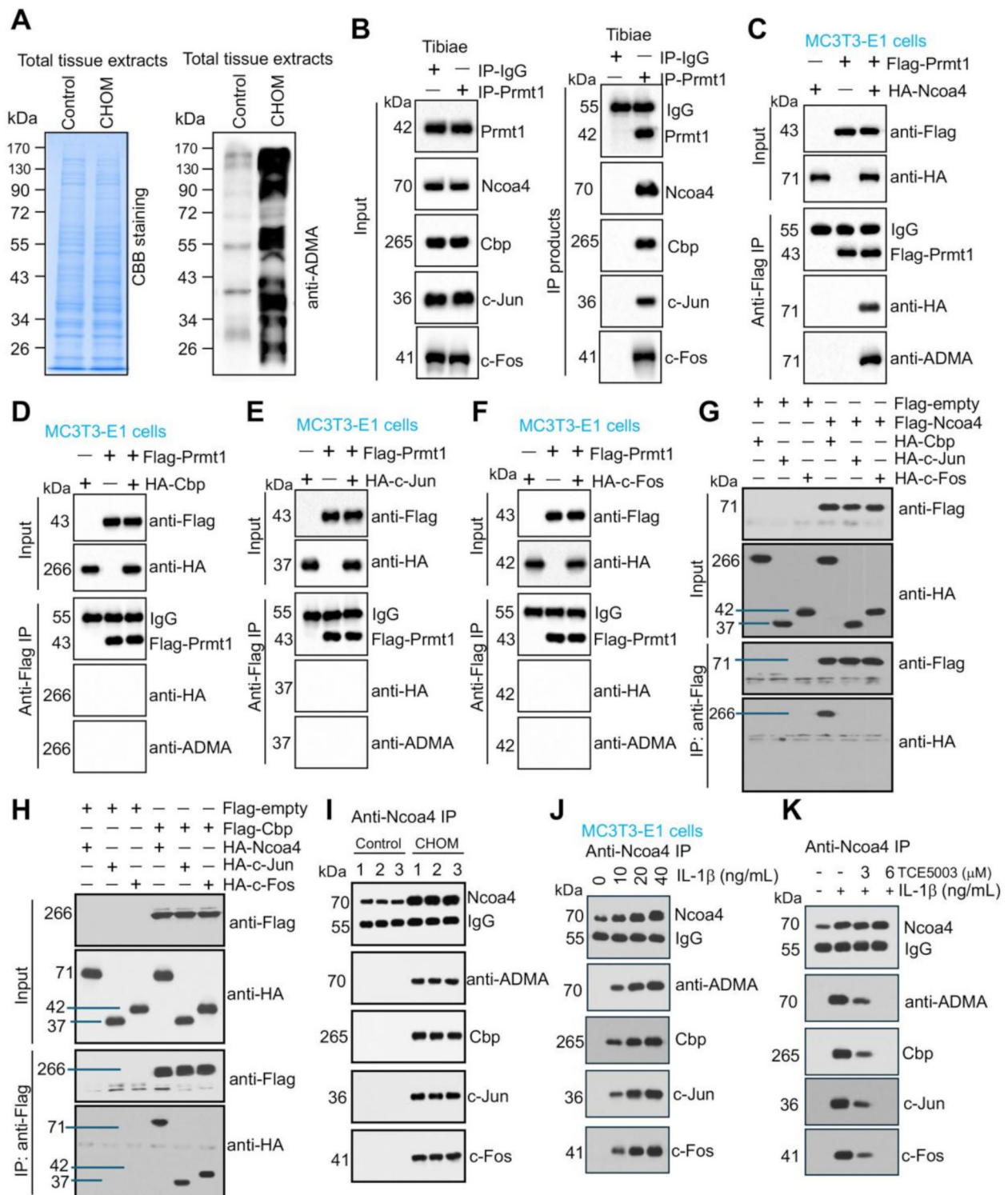


Fig. 3 (See legend on next page.)

tissues confirmed that Prmt1 could bind to NcoA4, Cbp, and Ap1 subunits (Fig. 3B).

To determine whether Prmt1 directly methylated NcoA4, Cbp, or Ap1 subunits, we co-transfected

MC3T3-E1 cells with Flag-Prmt1 and HA-tagged constructs of NcoA4, Cbp, c-Jun, or c-Fos, followed by co-IP assays to assess direct interactions and methylation levels. The results demonstrated that Prmt1 directly

(See figure on previous page.)

Fig. 3 Prmt1 methylated Ncoa4 and promoted the assembly of the Ncoa4-Cbp-Ap1 complex. **(A)** Total protein methylation levels in tibial tissue homogenates from Control and CHOM mice. Homogenates were prepared by mixing three independent tibiae of equal weight from the same groups of mice. Left panel: Coomassie Brilliant Blue (CBB) staining confirmed equal total protein loading. Right panel: Immunoblot analysis revealed global protein methylation levels. **(B)** Prmt1 interacted with Ncoa4, Cbp, and Ap1 subunits in vivo. Protein extracts from CHOM tibial tissues were immunoprecipitated using IgG and anti-Prmt1-conjugated protein G. Both input and immunoprecipitated samples were probed for Prmt1, Ncoa4, Cbp, c-Jun, and c-Fos. **(C)** Prmt1 interacted with Ncoa4 in vitro. MC3T3-E1 cells were co-transfected with Flag-Prmt1 and HA-Ncoa4. After 48 h, cells were lysed and immunoprecipitated using anti-Flag agarose. Input and immunoprecipitated samples were analyzed using anti-Flag, anti-HA, and anti-ADMA antibodies. **(D–F)** Determination of interactions between Prmt1 and Cbp **(D)**, Prmt1 and c-Jun **(E)**, and Prmt1 and c-Fos **(F)**. **(G)** Ncoa4 directly interacted with Cbp but not with Ap1 subunits in Co-IP assays. **(H)** Cbp directly interacted with both Ncoa4 and Ap1 subunits in Co-IP assays. **(I)** Ncoa4 immunoprecipitated Cbp and Ap1 subunits in CHOM tibial tissues. **(J)** Ncoa4 immunoprecipitated Cbp and Ap1 subunits in IL-1 β -treated MC3T3-E1 cells. **(K)** TCE-5003 treatment dose-dependently inhibited the assembly of the Ncoa4-Cbp-Ap1 complex

interacted with and methylated Ncoa4, but not Cbp or Ap1 subunits (Fig. 3C and F). These findings suggest that while Ncoa4 is a direct substrate for Prmt1-mediated methylation, the interactions of Cbp and Ap1 subunits with Prmt1 are likely indirect.

As Ncoa4 is a transcriptional coactivator, Cbp is a histone acetyltransferase, and Ap1 functions as a transcription factor [24, 25], we hypothesized that these proteins might form a functional complex. To test this, we co-transfected MC3T3-E1 cells with various combinations of Flag-Ncoa4, Myc-Cbp, Myc-c-Jun, and Myc-c-Fos. Co-IP experiments revealed that Ncoa4 directly interacted with Cbp but not with Ap1 subunits (Fig. 3G). In contrast, Cbp was found to directly interact with both Ncoa4 and Ap1 subunits (Fig. 3H).

We next performed IP assay using anti-Ncoa4-conjugated agarose beads on tibial tissue lysates from control and CHOM mice ($n=3$ per group). The results showed that arginine-methylated Ncoa4 was detectable only in CHOM tibiae, and that Ncoa4 formed complexes with Cbp, c-Jun, and c-FOS exclusively in this group (Fig. 3I). In a parallel experiment, MC3T3-E1 cells were treated with increasing concentrations of IL-1 β (0, 10, 20, and 40 ng/mL). IP was again performed using anti-Ncoa4-conjugated agarose beads to assess Ncoa4 arginine methylation and its interaction with Cbp, c-Jun, and c-FOS. We observed that both the protein level and the arginine methylation level of Ncoa4 increased in response to IL-1 β treatment. Furthermore, the levels of Cbp and AP-1 subunits co-precipitated with Ncoa4 also increased in an IL-1 β dose-dependent manner (Fig. 3J). Conversely, in MC3T3-E1 cells treated with TCE-5003 (0, 3, and 6 μ M) + 40 ng/mL IL-1 β or MS023 (0, 100, and 200 nM) + 40 ng/mL IL-1 β , the methylation level of Ncoa4, as well as the levels of Cbp and Ap1 subunits co-precipitated with Ncoa4, decreased in a dose-dependent manner (Figs. 3K and S6). In conclusion, our findings demonstrated that Prmt1 directly methylated Ncoa4. Inhibition of Prmt1 reduced Ncoa4 methylation, destabilized its protein levels, and disrupted its ability to form a functional complex with Cbp and Ap1. These results highlight the critical role of Prmt1-mediated methylation

in regulating the stability and assembly of the Ncoa4-Cbp-Ap1 transcriptional complex under inflammatory conditions.

Prmt1 catalyzed Ncoa4-ADMA at the R242 residue

To further identify the specific arginine methylation site on Ncoa4 catalyzed by Prmt1, we divided the full-length Ncoa4 protein (625 amino acids, aa) into three distinct regions: R1 (1–150 aa), R2 (151–450 aa), and R3 (451–625 aa) (Figs. 4A and S7). Using an in vitro methylation assay, we observed that only the full-length Ncoa4 and the R2 region were detectable with an anti-ADMA antibody, indicating that Prmt1-mediated methylation occurs specifically within the R2 region of Ncoa4 (Fig. 4B). To pinpoint the exact methylation site, we systematically mutated all arginine (R) residues within the R2 region to lysine (K), generating the following mutants: R182K, R242K, R342K, and R366K. The in vitro methylation assay demonstrated that Prmt1 was unable to methylate the R242K mutant, while methylation of R182K, R342K, and R366K remained unaffected (Fig. 4C). This finding strongly suggested that Prmt1 catalyzed ADMA of Ncoa4 specifically at the R242 residue.

To further validate this result, we constructed HA-tagged Ncoa4 variants, including HA-Ncoa4^{WT}, HA-Ncoa4^{R182K}, HA-Ncoa4^{R242K}, HA-Ncoa4^{R342K}, and HA-Ncoa4^{R366K}, and co-transfected them with Flag-Prmt1 into MC3T3-E1 cells. IP assays using anti-Flag agarose revealed a significant reduction in ADMA-modified Ncoa4 levels in the R242K mutant compared to the WT control (Fig. 4D). In contrast, the ADMA modification levels in the R182K, R342K, and R366K mutants were comparable to those in the WT group (Fig. 4D). These results provide compelling evidence that Prmt1 specifically catalyzes the ADMA modification of Ncoa4 at the R242 residue (Fig. 4D).

Ncoa4 was ubiquitinated by Rnf8 E3 ligase in IL-1 β -treated cells with Prmt1 knockdown or inhibition

In Figs. 2 and S5, we observed a reduction in Ncoa4 protein level in MC3T3-E1 cells treated with IL-1 β when Prmt1 was knocked down or inhibited by Prmt1 inhibitors. This suggests that Ncoa4 may undergo degradation

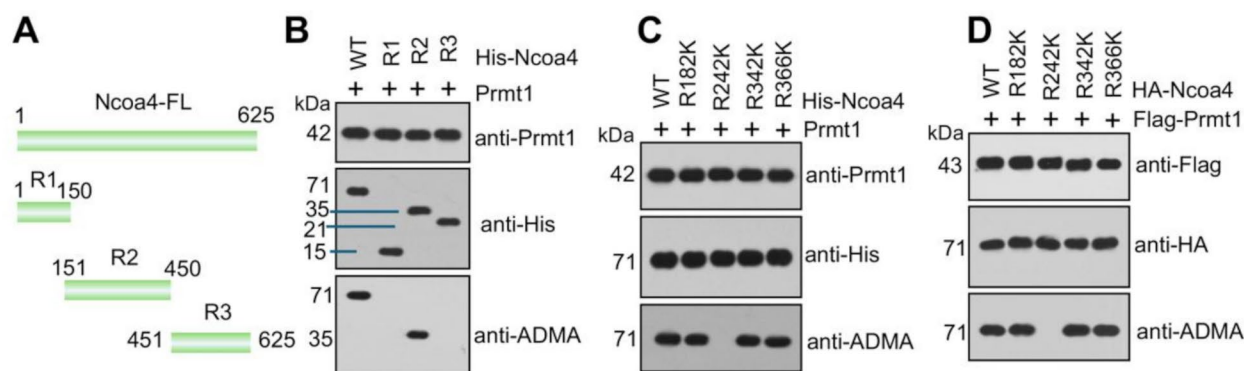


Fig. 4 Prmt1 methylated Ncoa4 at the R242 residue. **(A)** Different regions of the Ncoa4 protein: R1 (1–150 aa), R2 (151–450 aa), and R3 (451–625 aa). **(B)** Prmt1 methylated the R2 region of Ncoa4 in vitro. An in vitro methylation assay was performed using recombinant Prmt1 and His-Ncoa4, His-Ncoa4^{R1}, His-Ncoa4^{R2}, and His-Ncoa4^{R3}. Immunoblots were conducted using anti-ADMA, anti-His, and anti-Prmt1 antibodies. **(C)** Prmt1 methylated the R242 residue of Ncoa4. An in vitro methylation assay was performed using recombinant Prmt1 and His-Ncoa4 or its mutants (Ncoa4^{R182K}, Ncoa4^{R242K}, Ncoa4^{R342K}, or Ncoa4^{R366K}). Immunoblots were conducted using anti-ADMA, anti-His, and anti-Prmt1 antibodies. **(D)** Prmt1 methylated the R242 residue of Ncoa4 in MC3T3-E1 cells. MC3T3-E1 cells were co-transfected with Flag-Prmt1 and HA-Ncoa4 or its mutants (Ncoa4^{R182K}, Ncoa4^{R242K}, Ncoa4^{R342K}, or Ncoa4^{R366K}). Forty-eight hours after transfection, the cells were lysed and immunoprecipitated with anti-Flag agarose, followed by immunoblot analyses using anti-Flag, anti-Ncoa4, and anti-ADMA antibodies

when Prmt1 function is impaired. Given that ubiquitination-mediated proteasomal degradation is the most common degradation pathway, we hypothesized that Ncoa4 might be ubiquitinated in Prmt1^{KD} cells upon IL-1 β treatment. To test this hypothesis, we co-treated Prmt1^{KD} cells with 40 ng/mL IL-1 β and MG132 (a proteasome inhibitor), as well as cells co-treated MC3T3-E1 cells with IL-1 β , TCE-5003 (or MS023), and MG132. IP assay was then performed using anti-Ncoa4-conjugated agarose beads to assess whether Ncoa4 underwent ubiquitination. The results demonstrated that Ncoa4 was ubiquitinated when Prmt1 was knocked down or inhibited, whereas no ubiquitination of Ncoa4 was observed in IL-1 β -treated Control^{KD} cells (Fig. 5A and B). Furthermore, in MG132-treated cells, the levels of Ncoa4 ubiquitination were significantly elevated (Fig. 5A and B), underscoring the role of proteasomal degradation in regulating Ncoa4 stability. We also performed IP assay using anti-Ncoa4-conjugated agarose beads on tibial tissue lysates from control and CHOM mice ($n=3$ per group), followed by detection of Ncoa4 ubiquitination. The results showed that ubiquitinated Ncoa4 was undetectable in the tibial tissues of both control and CHOM mice (Fig. 5C).

To further investigate the mechanism of Ncoa4 ubiquitination, we performed IP followed by mass spectrometry analysis in MG132- and IL-1 β -treated Prmt1^{KD} cells using anti-Ncoa4. This revealed a significant enrichment of the E3 ubiquitin ligase Rnf8 in the anti-Ncoa4 IP products (Table S8). Subsequent IP experiments confirmed interaction between Ncoa4 and Rnf8 (Fig. 5D and E).

Given that Rnf8 is an E3 ubiquitin ligase, we conducted in vitro ubiquitination assays to examine whether

GST-Rnf8 could ubiquitinate His-tagged Ncoa4 fragments, including His-Ncoa4^{R1(1–150)}, His-Ncoa4^{R2(151–450)}, and His-Ncoa4^{R3(451–625)}. The results showed that GST-Rnf8 ubiquitinated both His-Ncoa4^{WT} and His-Ncoa4^{R1} (Fig. 5F). To identify the specific ubiquitination site within the R1 region, we generated point mutations at all lysine (K) residues, including K42A, K49A, K81A, K112A, and K131A. In vitro ubiquitination assays revealed that Rnf8 failed to ubiquitinate the Ncoa4^{K49A} mutant, while ubiquitination of Ncoa4^{K42A}, Ncoa4^{K81A}, Ncoa4^{K112A}, and Ncoa4^{K131A} remained unaffected (Fig. 5G). This indicates that K49 is the specific ubiquitination site on Ncoa4 targeted by Rnf8. To further validate these findings, we constructed HA-tagged Ncoa4 variants, including HA-Ncoa4^{WT}, HA-Ncoa4^{K42A}, HA-Ncoa4^{K49A}, HA-Ncoa4^{K81A}, HA-Ncoa4^{K112A}, and HA-Ncoa4^{K131A}, and co-transfected them with Flag-Rnf8 into MC3T3-E1 cells. IP assays using anti-HA agarose demonstrated that ubiquitinated Ncoa4 was absent in the K49A mutant (Fig. 5H). In contrast, the ubiquitination levels of the K42A, K81A, K112A, and K131A mutants were comparable to those of the WT group (Fig. 5H). These results provide compelling evidence that Rnf8 specifically ubiquitinates Ncoa4 at the K49 residue (Fig. 5H).

The Ncoa4-Cbp-Ap1 complex regulated the expression of *Adamts3/8/12/14* genes

In Fig. 2, we observed that the expression of *Adamts3/8/12/14* was dependent on Prmt1. Furthermore, the expression levels of these *Adamts* genes in both Control^{KD} and Prmt1^{KD} cells, regardless of IL-1 β treatment, were entirely consistent with those of Ncoa4. Moreover, we identified that all *Adamts3/8/12/14*

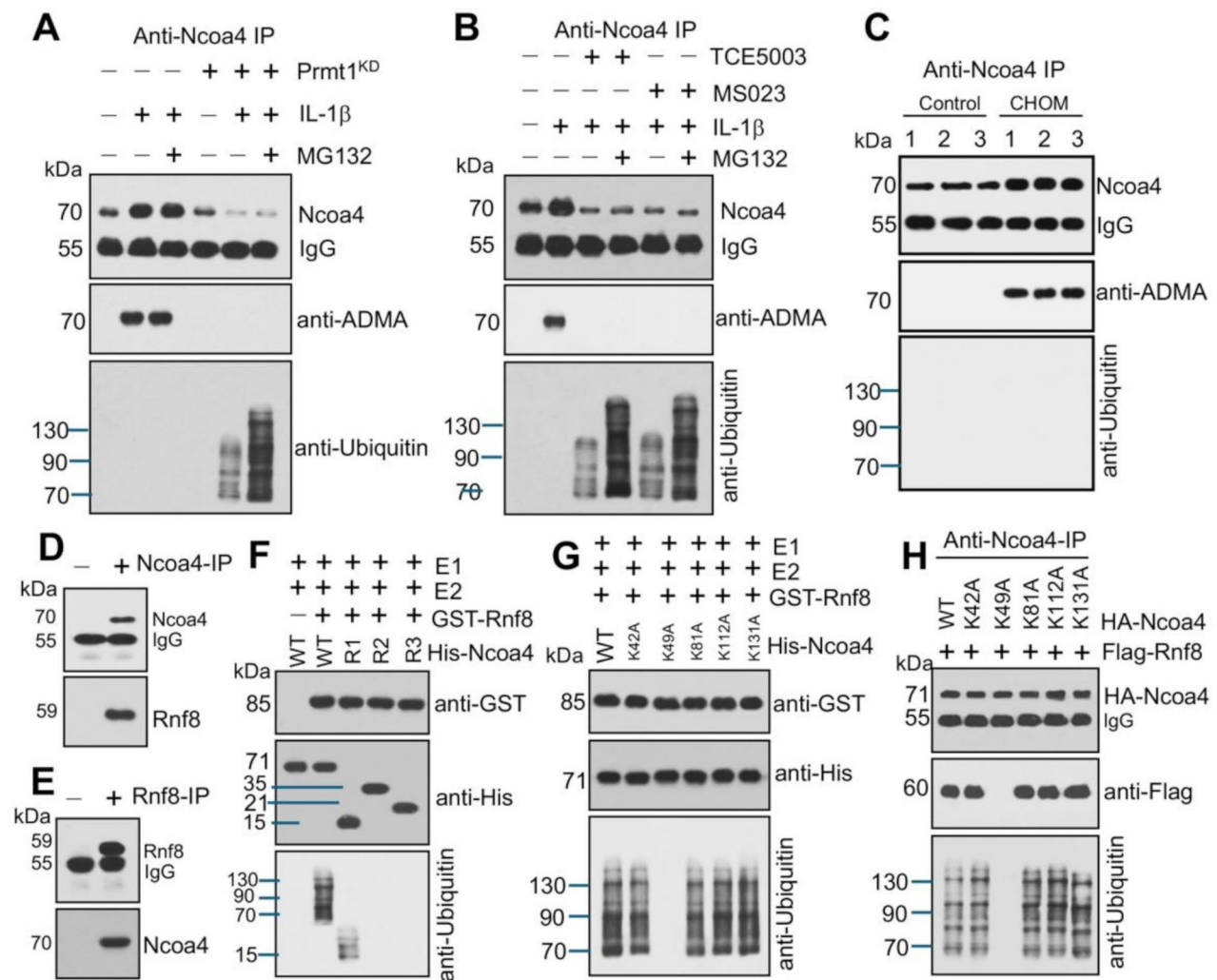


Fig. 5 Rnf8 ubiquitinated Ncoa4 at the K49 residue. **(A)** Effects of IL-1 β and MG132 on Ncoa4 methylation and ubiquitination in Prmt1^{KD} cells. Prmt1^{KD} cells were treated with IL-1 β alone or co-treated with IL-1 β and MG132 for 6 h, followed by an IP assay using anti-Ncoa4 agarose. The purified proteins were probed with anti-Ncoa4, anti-ADMA, and anti-Ubiquitin antibodies. **(B)** Effects of IL-1 β , TCE-5003 (or MS023), and MG132 on Ncoa4 methylation and ubiquitination in MC3T3-E1 cells. MC3T3-E1 cells were treated with IL-1 β alone, co-treated with IL-1 β and TCE-5003 (or MS023), or co-treated with IL-1 β , TCE-5003 (or MS023), and MG132 for 6 h, followed by an IP assay using anti-Ncoa4 agarose. The purified proteins were probed with anti-Ncoa4, anti-ADMA, and anti-Ubiquitin antibodies. **(C)** Ncoa4 underwent arginine methylation, but not ubiquitination, in CHOM tibial tissues. Tibial tissues from control and CHOM mice ($n=3$ per group) were subjected to IP assay using anti-Ncoa4-conjugated agarose beads. The IP products were analyzed by immunoblotting with anti-Ncoa4, anti-ADMA, and anti-Ubiquitin antibodies. **(D)** and **(E)** Rnf8 interacted with Ncoa4 in Prmt1^{KD} cells. The Prmt1^{KD} cells were lysed and immunoprecipitated using anti-Ncoa4 agarose **(D)** or anti-Rnf8 agarose **(E)**. The purified proteins were probed with anti-Rnf8 and anti-Ncoa4 antibodies. **(F)** Rnf8 ubiquitinated the Ncoa4^{R1} region in vitro. An in vitro ubiquitination assay was performed using E1, E2, recombinant GST-Rnf8, and His-Ncoa4 or its truncated mutants (Ncoa4^{R1}, Ncoa4^{R2}, and Ncoa4^{R3}). Immunoblots were conducted using anti-GST, anti-His, and anti-Ubiquitin antibodies. **(G)** Rnf8 ubiquitinated Ncoa4 at the K49 residue in vitro. An in vitro ubiquitination assay was performed using recombinant GST-Rnf8 and His-Ncoa4 or its mutants (Ncoa4^{K42A}, Ncoa4^{K49A}, Ncoa4^{K81A}, Ncoa4^{K112A}, or Ncoa4^{K131A}). Immunoblots were conducted using anti-GST, anti-His, and anti-Ubiquitin antibodies. **(H)** RNF8 ubiquitinated Ncoa4 at the K49 residue in MC3T3-E1 cells. MC3T3-E1 cells were co-transfected with Flag-Rnf8 and HA-Ncoa4 or its mutants (Ncoa4^{K42A}, Ncoa4^{K49A}, Ncoa4^{K81A}, Ncoa4^{K112A}, or Ncoa4^{K131A}). Forty-eight hours after transfection, the cells were lysed and immunoprecipitated with anti-Ncoa4 agarose, followed by immunoblot analyses using anti-Flag, anti-HA, and anti-Ubiquitin antibodies

promoters (2,500 bp in length) contained one or two Ap1-binding sites (TGAG/CTCA) (Fig. 6A). Thus, we hypothesize that the Ncoa4-Cbp-Ap1 complex may regulate the expression of *Adamts3/8/12/14* at the transcriptional level, thereby influencing the expression of the proteins encoded by these four genes. To test this hypothesis, we

established Control^{KD}, Ncoa4^{KD}, Cbp^{KD}, c-Jun^{KD}, and c-Fos^{KD} cell lines in MC3T3-E1 cells (Fig. 6B). We then measured the expression of *Adamts3/8/12/14* genes and the enrichment levels of the Ncoa4-Cbp-Ap1 complex members at the promoter regions of these genes under both IL-1 β -treated (40 ng/mL) and untreated conditions.

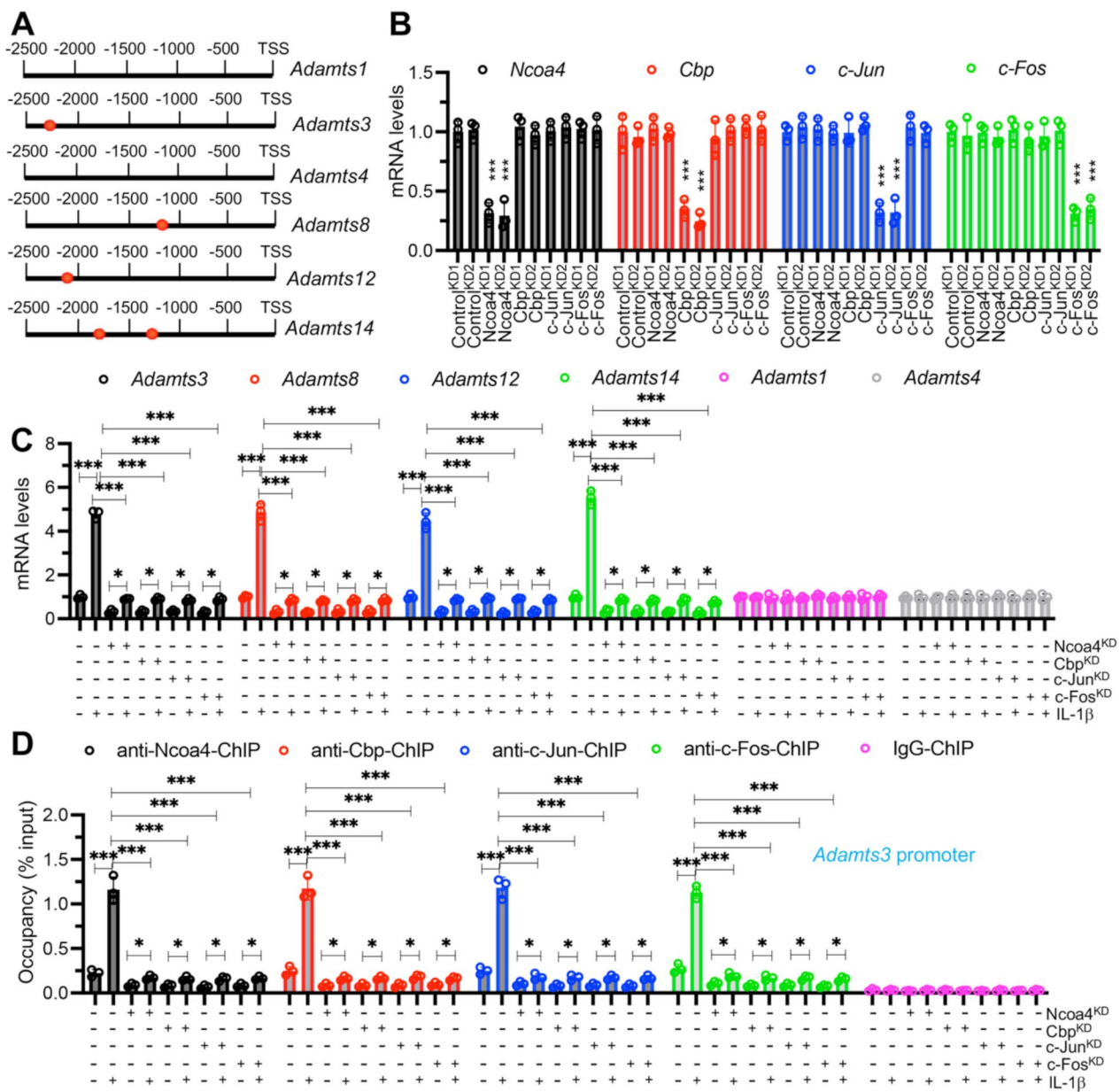


Fig. 6 Knockdown of Nco4-Cbp-Ap1 components reduced the expression of *Adamts3/8/12/14*. **(A)** Schematic representation of Ap1 transcription factor binding sites on *Adamts1/3/4/8/12/14* promoters (2500 bp length). **(B)** Quantitative analysis of *Nco4*, *Cbp*, *c-Jun*, and *c-Fos* mRNA expression levels in MC3T3-E1 cells following knockdown experiments (Control^{KD1/2}, Nco4^{KD1/2}, Cbp^{KD1/2}, c-Jun^{KD1/2}, and c-Fos^{KD1/2}). **(C)** Quantitative mRNA expression profiles of *Adamts1/3/4/8/12/14* in Control^{KD1}, Nco4^{KD1}, Cbp^{KD1}, c-Jun^{KD1}, and c-Fos^{KD1} cells treated with or without IL-1β (40 ng/mL). **(D)** ChIP analysis. Cells from **(C)** were subjected to ChIP assays using specific antibodies against Nco4, Cbp, c-Jun, c-Fos, and IgG-conjugated protein G agarose. Enrichment of Nco4-Cbp-Ap1 components on the promoter of *Adamts3* was quantified by RT-qPCR analysis of input and immunoprecipitated DNA samples. **P* < 0.05, ****P* < 0.001

Compared with IL-1β-treated Control^{KD} cells, the expression of *Adamts3/8/12/14* was significantly reduced in IL-1β-treated cells with knockdown of the Nco4-Cbp-AP-1 complex (Fig. 6C). In addition, we examined the effects of depleting components of the Nco4-Cbp-AP-1 complex, as well as IL-1β treatment, on the expression of *Adamts1* and *Adamts4*—two genes whose promoters lack Ap1 binding sites (Fig. 6A). The results showed that

knockdown of Nco4-Cbp-AP-1 complex members did not alter the expression levels of *Adamts1* or *Adamts4*, regardless of IL-1β treatment (Fig. 6C). These findings further confirmed that the Nco4-Cbp-AP-1 complex specifically regulated *Adamts3/8/12/14* genes, but not genes lacking AP1 binding sites.

ChIP assays demonstrated that the Nco4-Cbp-AP-1 complex bound to the promoter regions of

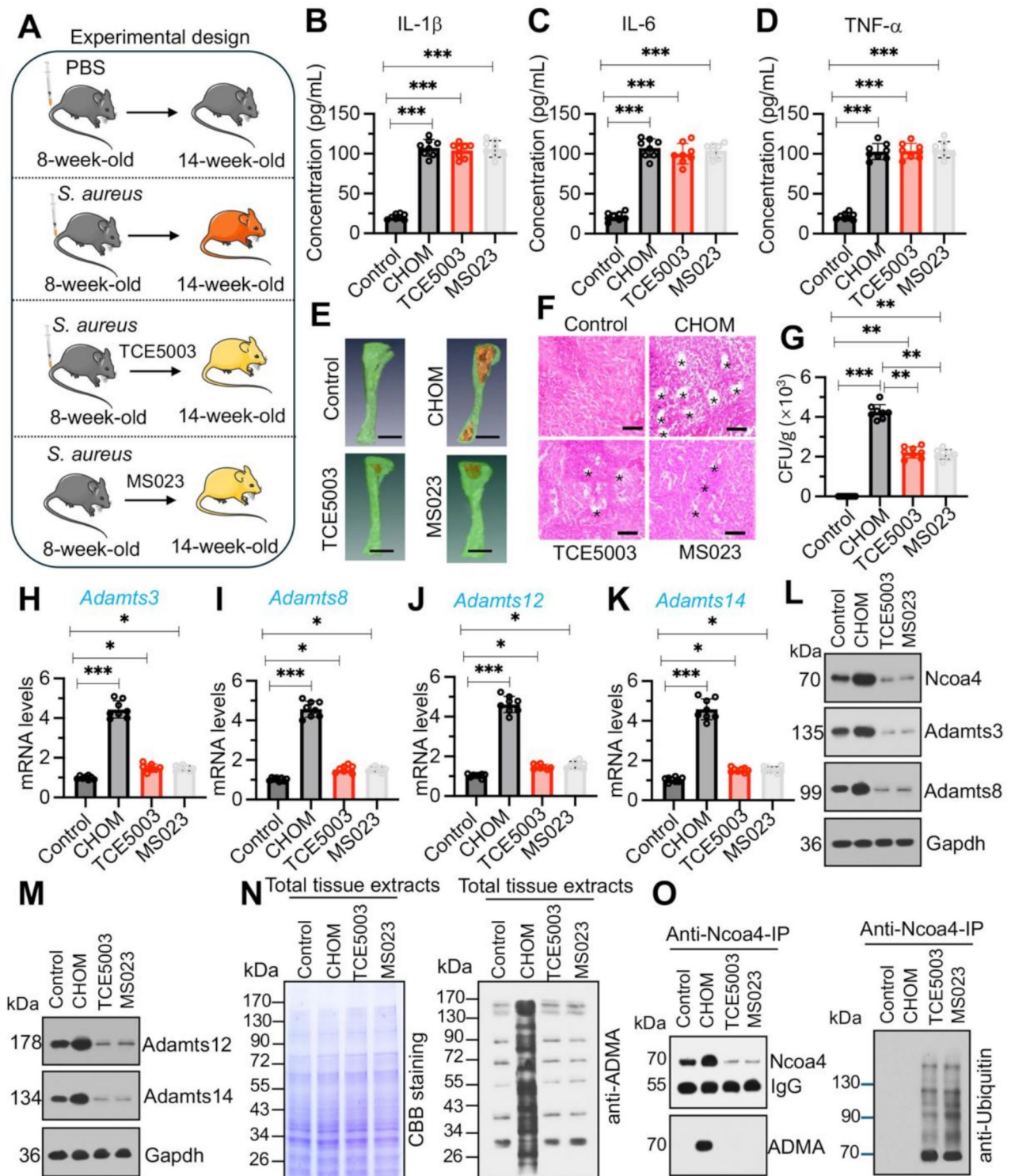


Fig. 7 (See legend on next page.)

Adamts3/8/12/14 genes, and its enrichment levels were significantly upregulated by IL-1 β in Control^{KD} cells (Figs. 6D, S8 and S9). Knockdown of any single member of the complex led to a marked decrease in

the enrichment levels of the other members at the promoter regions of *Adamts3/8/12/14* genes (Figs. 6D and S8). In IL-1 β -treated knockdown cell lines of the Ncoa4-Cbp-Ap1 complex members, the enrichment

(See figure on previous page.)

Fig. 7 Inhibitors of Prmt1 attenuated CHOM progression. **(A)** Experimental design schematic showing the four groups of mice: Control, CHOM, TCE-5003-treated, and MS023-treated. **(B–D)** Serum cytokine levels of IL-1 β **(B)**, IL-6 **(C)**, and TNF- α **(D)** in Control, CHOM, TCE-5003, and MS023 groups ($n=8$ per group). **(E)** Representative images of tibial inflammatory lesions in Control, CHOM, TCE-5003, and MS023 groups. **(F)** Representative H&E-stained sections of tibiae from Control, CHOM, TCE-5003, and MS023 groups. Asterisks (*) indicated areas of sequestrum formation. **(G)** Quantification of bacterial load in tibiae. Homogenates from 1 g of tibial tissue were plated on TSA plates, incubated at 37 °C for 20 h, and CFUs were enumerated. **(H–K)** mRNA expression levels of *Adamts3* **(H)**, *Adamts8* **(I)**, *Adamts12* **(J)**, and *Adamts14* **(K)** in tibial tissues from Control, CHOM, TCE-5003, and MS023 groups ($n=8$ per group). **(L and M)** Western blot analysis of Ncoa4, Adamts3, and Adamts8 **(L)**, as well as Adamts12 and Adamts14 **(M)** protein levels in tibial tissues from Control, CHOM, TCE-5003, and MS023 groups ($n=3$ per group). **(N)** Total protein methylation levels in tibial tissue homogenates from Control, CHOM, TCE-5003, and MS023 mice. Homogenates were prepared by mixing three independent tibiae of equal weight from the same groups of mice. Left panel: CBB staining confirmed equal total protein loading. Right panel: Immunoblot analysis revealed global protein methylation levels. **(O)** Effects of TCE-5003 and MS023 treatment on Ncoa4 methylation and ubiquitination levels. Tibial tissues from control, CHOM, TCE-5003, and MS023 groups ($n=3$ per group; tissues from each group were pooled in equal weights prior to the IP assay) were subjected to immunoprecipitation using anti-Ncoa4-conjugated agarose beads. The immunoprecipitated proteins were analyzed by immunoblotting with anti-Ncoa4, anti-ADMA, and anti-Ubiquitin antibodies. * $P<0.05$; ** $P<0.01$; *** $P<0.001$

levels of Ncoa4, Cbp, and Ap1 subunits at the promoter regions of *Adamts3/8/12/14* genes were only marginally upregulated compared to untreated cells (Figs. 6D and S8). Furthermore, we examined the occupancy of the Ncoa4–Cbp–Ap1 complex at the promoters of *Adamts1* and *Adamts4*, which lack canonical Ap1 binding sites. The complex showed no detectable binding to either promoter, regardless of IL-1 β treatment (Figure S9). Collectively, these findings demonstrate that the Ncoa4–Cbp–Ap1 complex plays a critical and specific role in the IL-1 β –responsive transcriptional regulation of *Adamts3/8/12/14*.

Treatments with Prmt1 inhibitors effectively suppressed IL-1 β -induced *Adamts* expression in vitro

Given the critical role of Ncoa4 in regulating the expression of *Adamts3/8/12/14*, we hypothesized that Prmt1 inhibition in an inflammatory microenvironment could suppress Ncoa4-mediated transcription of these genes. To test this, we treated MC3T3-E1 cells with increasing concentrations of TCE-5003 (0, 3, and 6 μ M) and MS023 (0, 100, and 200 nM) in combination with 40 ng/mL IL-1 β . The results demonstrated that both TCE-5003 and MS023 treatment led to a dose-dependent suppression of *Adamts3/8/12/14* expression (Figures S10A). ChIP assays also indicated that TCE-5003 and MS023 could dose-dependently inhibited the binding of Ncoa4, Cbp, and Ap1 subunits at the promoter regions of *Adamts3/8/12/14* genes (Figures S10B, S10C, and S11).

Administration of Prmt1 inhibitors in *S. aureus*-injected mice significantly prevented the incidence of CHOM

The promising effects of Prmt1 inhibitors in reducing IL-1 β -induced *Adamts3/8/12/14* expression prompted us to investigate their in vivo efficacy in preventing CHOM. To this end, we randomly assigned mice into four groups: PBS (Control), *S. aureus* (CHOM), *S. aureus* + 50 mg/kg TCE-5003 (TCE-5003), and *S. aureus* + 50 mg/kg MS023 (MS023) ($n=8$ per group) (Fig. 7A).

Six weeks post-injection, ELISA results showed that the circulating levels of IL-1 β , IL-6, and TNF- α were

significantly elevated in the CHOM, TCE-5003, and MS023 groups compared to the control group (Fig. 7B and D). However, the cytokine levels were comparable among the CHOM, TCE-5003, and MS023 groups, with no significant differences observed between them (Fig. 7B and D). Inflammatory lesions in the tibiae were markedly reduced in the TCE-5003 and MS023 groups compared to the CHOM group (Fig. 7E). H&E staining further demonstrated that bone destruction was significantly inhibited in the TCE-5003 and MS023 groups compared to CHOM mice (Fig. 7F). Additionally, CFU assays of tibia homogenates showed a significantly decreased bacterial load of *S. aureus* in TCE-5003 and MS023 groups compared to CHOM mice (Fig. 7G).

To further assess the molecular effects of Prmt1 inhibition, we examined the mRNA and protein levels of *Adamts3/8/12/14* in tibial tissues across all groups. Compared to the Control group, the CHOM group exhibited increased expression of these genes and proteins (Fig. 7H and M). However, in the TCE-5003 and MS023 groups, the expression levels of *Adamts3/8/12/14* were significantly reduced compared to the CHOM group (Fig. 7H and M). We also assessed global arginine methylation levels in total tibial tissue lysates from the four groups of mice. The results showed that treatment with TCE-5003 and MS023 significantly reduced methylation signal intensity, bringing it to levels comparable to those observed in control mice (Fig. 7N). Moreover, we conducted IP assay using anti-Ncoa4-conjugated agarose beads on tibial tissue lysates from control, CHOM, TCE-5003, and MS023-treated mice. We then examined the arginine methylation and ubiquitination status of Ncoa4. The results showed that arginine methylation of Ncoa4 was undetectable in the tibial tissues of TCE-5003- and MS023-treated mice (Fig. 7O). In contrast, Ncoa4 ubiquitination was clearly detected in both treatment groups (Fig. 7N). These findings are consistent with our in vitro observations (Fig. 5A and B), indicating that under inflammatory conditions, inhibition of Prmt1 leads to a loss of Ncoa4 methylation, rendering it susceptible to ubiquitin-mediated degradation. Collectively, these

results suggest that TCE-5003 and MS023 may effectively prevent CHOM development in *S. aureus*-infected mice by downregulating Adamts expression, thereby alleviating inflammation-induced bone destruction.

Discussion

Bone ECM degradation is a key driver of osteomyelitis pathogenesis, as it provides structural support and regulates various cellular functions within bone tissue [13, 14]. During osteomyelitis, ECM integrity is disrupted due to the upregulation of Mmps and Adamts proteins. While Adamts are known to contribute to osteomyelitis by promoting ECM degradation in osteoblasts, the expression patterns of its 19 family members, the upstream signaling pathways responsible for their overexpression, and their cellular sources remain unclear. In this study, we established a CHOM mouse model infected with *S. aureus* and identified Prmt1 as a key regulator highly expressed in infected tibial tissues. In vitro experiments revealed that Prmt1 was specifically expressed in osteoblasts and osteocytes, but not in osteoclasts or bone marrow macrophages, indicating its primary cellular sources in the bone microenvironment. Mechanistically, we demonstrated that Prmt1 directly methylates Ncoa4 at R242, stabilizing its protein levels. Methylated Ncoa4 then forms a transcriptional complex with Cbp and Ap1, which binds to the promoter regions of *Adamts3/8/12/14*, driving their transcription. Overexpression of these Adamts enzymes enhances ECM degradation, contributing to bone destruction and CHOM progression (Fig. 8A). Pharmacological inhibition of Prmt1 with TCE-5003 and MS023 reduced Ncoa4 methylation, leading to its ubiquitination and subsequent proteasomal degradation by Rnf8 E3 ligase within the inflammatory microenvironment. This resulted in the disassembly of the Ncoa4–Cbp–Ap1 complex, suppression of *Adamts3/8/12/14* transcription, inhibition of ECM degradation, and ultimately prevention of bone destruction in CHOM (Fig. 8B).

Prmts play essential roles in gene expression, RNA metabolism, signal transduction, and protein stability, with their dysregulation implicated in various diseases, including cancer, neurodegeneration, autoimmune disorders, and infections [16, 17]. Among Prmt family members, Prmt1, Prmt4, and Prmt5 are particularly notable for modifying key regulatory proteins such as p53 [18], Foxo1 [19], and Stat3 (Signal transducer and activator of transcription 3) [26], thereby influencing tumor progression, immune responses, and inflammatory signaling. Our study is the first to establish Prmt1 as a key regulator in CHOM development. Among all Prmt family members, only Prmt1 was significantly upregulated in CHOM-afflicted tibial tissues, suggesting its specific involvement in disease progression. A pivotal finding of our study is that Prmt1 directly methylates Ncoa4 at

R242, a modification crucial for preventing its ubiquitination and subsequent proteasomal degradation. In the absence of Prmt1 activity, Rnf8 E3 ubiquitin ligase ubiquitinates Ncoa4 at K49, leading to its degradation. This highlights a novel interplay between methylation and ubiquitination in controlling protein stability under inflammatory conditions. Arginine methylation and ubiquitination of Ncoa4 are two distinct and mutually exclusive processes. In an inflammatory microenvironment, Ncoa4 undergoes arginine methylation by Prmt1, which preserves its protein stability—a key mechanism promoting CHOM development. However, when Prmt1 function is inhibited, Ncoa4 fails to be methylated and consequently loses its protective modification. This unmethylated form of Ncoa4 is then recognized by Rnf8, leading to its ubiquitination and subsequent degradation. This regulatory switch represents a critical strategy for suppressing CHOM development and progression.

In addition to Rnf8, Herc2 has been reported to mediate Ncoa4 ubiquitination in an iron-dependent manner during erythropoiesis. It is well established that different E3 ligases can target the same substrate depending on the biological processes or cellular environment. For example, p53 can be ubiquitinated by Mdm2 (Mouse double minute 2) [27], Ring1 (Ring finger protein 1) [28], and Trim24 (Tripartite motif-containing 24) [29], whereas I κ B α (NF κ B Inhibitor alpha) is targeted by β -TrCP (Beta-transducin repeat containing E3 ligase) [30], and Keap1 (Kelch like ECH associated protein 1) [31]. In our study, immunoprecipitation followed by mass spectrometry in MG132- and IL-1 β -treated Prmt1 knockdown osteoblasts identified Rnf8 as a direct Ncoa4-interacting protein, while Herc2 was not detected in our proteomic analysis. Although we cannot completely rule out the potential involvement of Herc2, these findings suggest that it likely plays a minimal or non-essential role in regulating Ncoa4 under inflammatory conditions associated with osteomyelitis. Future studies will investigate whether Herc2 contributes to Ncoa4 ubiquitination in the pathogenesis of osteomyelitis.

Moreover, we reveal that Ncoa4 functions as a transcriptional coactivator, its degradation in Prmt1-deficient conditions results in impaired transcription of ECM-degrading enzymes, ultimately affecting osteoblast function and bone remodeling. This mechanism aligns with previous studies demonstrating that Prmt-mediated methylation regulates protein stability in various biological contexts. For example, Prmt1 methylation of Rbm15^{R578} (RNA binding motif protein 15) leads to its degradation via ubiquitylation by Cnot4 (CCR4-NOT transcription complex subunit 4) E3 ligase [32], while Usp11 (Ubiquitin specific peptidase 11) is methylated by Prmt1 at R433, promoting DNA damage repair [33]. Similarly, Prmt5 methylation of Pdgfra (Platelet derived

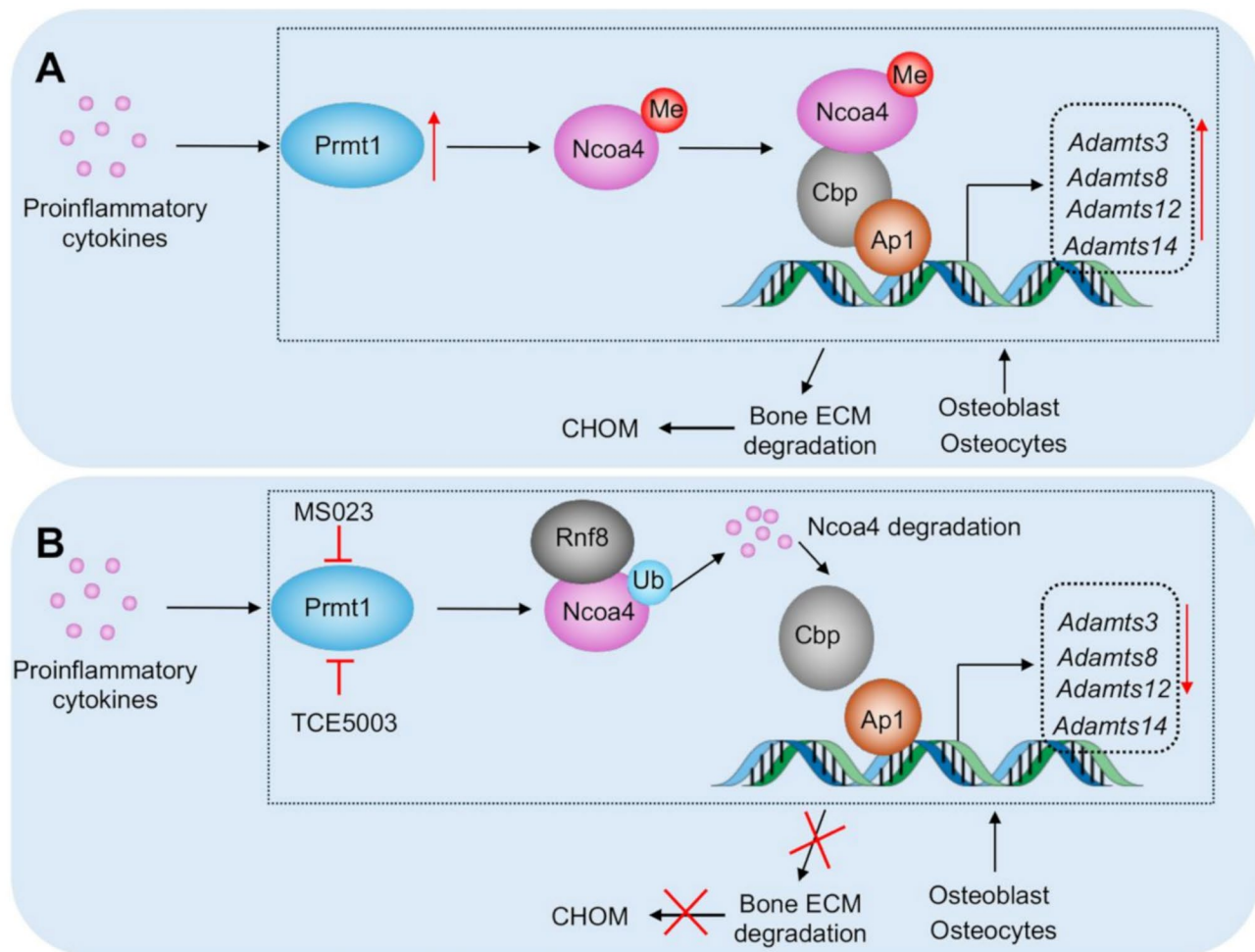


Fig. 8 Schematic models of the Prmt1/Ncoa4-Cbp-Ap1/Adamts signaling axis in CHOM pathogenesis and its therapeutic inhibition. **(A)** Mechanism of Prmt1/Ncoa4-Cbp-Ap1/Adamts axis in CHOM pathogenesis. Upon *S. aureus* infection, proinflammatory cytokines upregulate Prmt1 expression in osteoblasts and osteocytes. Prmt1 catalyzes the methylation of Ncoa4, enhancing its stability. Methylated Ncoa4 forms a transcriptional complex with Cbp and Ap1 subunits, which binds to the promoters of *Adamts3/8/12/14*, driving their transcriptional activation. The upregulation of Adamts proteins promotes bone ECM degradation, leading to bone destruction and the development of CHOM. **(B)** Therapeutic inhibition of Prmt1 to prevent CHOM progression. Treatment with Prmt1 inhibitors (TCE-5003 and MS023) suppresses Ncoa4 methylation. Unmethylated Ncoa4 is ubiquitinated by the E3 ligase Rnf8 and subsequently degraded via the proteasome pathway. This degradation disrupts the Ncoa4-Cbp-Ap1 transcriptional complex, leading to the downregulation of *Adamts3/8/12/14* expression. Consequently, bone ECM degradation is attenuated, preventing bone destruction and halting CHOM progression.

growth factor receptor alpha) at R554 prevents its degradation via Cbl E3 ligase, playing a role in oligodendrocyte differentiation and myelination [34]. These findings suggest that Prmt1-mediated protein stabilization extends beyond CHOM, potentially influencing other inflammatory and degenerative bone disorders.

The Adamts family of proteases plays a critical role in various disease models, including arthritis, intervertebral disc degeneration (IDD), acute respiratory distress syndrome (ARDS), cancer, and cardiovascular diseases, with distinct expression patterns observed across different biological processes. For instance, Adamts7 and Adamts12 are involved in the pathogenesis of arthritis [35]. Adamts1/3/4/5/7/12/15 are upregulated in IDD [36], while Adamts4 overexpression is linked to ARDS

[37]. Emerging research highlights the cardiovascular roles of Adamts proteases, particularly in vascular and cardiac development, including heart valve formation, with Adamts1/4/5 implicated in cardiovascular disease [38]. To date, 10 of the 19 Adamts members (Adamts1, 2, 4, 5, 8, 9, 12, 13, 15, and 18) have been shown to regulate angiogenesis and/or cancer progression [39], though the mechanisms underlying Adamts dysregulation remain unclear. In this study, we demonstrate that the Ncoa4-Cbp-Ap1 transcriptional complex specifically transactivates *Adamts3/8/12/14* genes, providing insights into Adamts overexpression and its role in the pathogenesis of CHOM. Our findings not only delineate the expression patterns of Adamts proteases in the pathogenesis

of CHOM but also provide mechanistic insights into the overexpression of Adamts.

Recent advancements in osteomyelitis treatment encompass both conventional and innovative approaches. Traditional methods, such as long-term antibiotic therapy and surgical debridement, remain the cornerstone of management, while novel strategies, including localized drug delivery systems, biocompatible materials, immunotherapy, and bacteriophage therapy, have emerged as promising alternatives [2, 40]. Localized drug delivery systems, such as antibiotic-impregnated beads, enable high local antibiotic concentrations while minimizing systemic toxicity [2, 40]. Additionally, immunotherapy and bacteriophage therapy offer potential solutions for combating antibiotic-resistant infections [2, 40]. However, in clinical settings, the use of antibiotics, immunotherapy, or bacteriophage therapy alone is often insufficient to fully prevent osteomyelitis progression and associated bone destruction [2, 40]. In this study, we identified Prmt1 inhibition as a novel therapeutic approach for osteomyelitis, demonstrating that suppressing Prmt1 effectively downregulates Adamts expression and prevents disease progression, which holds significant clinical implications. Pharmacological inhibition of Prmt1 using TCE-5003 and MS023 effectively suppressed Ncoa4 methylation, destabilized the Ncoa4-Cbp-Ap1 transcriptional complex, and downregulated Adamts3/8/12/14, thereby mitigating ECM degradation and inflammatory bone destruction. Based on these findings, future osteomyelitis treatment strategies may require an integrated approach that combines antibiotic therapy, immunotherapy, bacteriophage therapy, and adjunctive therapies targeting bone ECM degradation to enhance therapeutic efficacy and improve patient outcomes.

In conclusion, this study identifies Prmt1 as a critical regulator of CHOM progression, functioning through Ncoa4 methylation and stabilization to drive Adamts3/8/12/14 expression and ECM degradation. By targeting Prmt1, we demonstrated that bone destruction and disease severity could be significantly mitigated, providing a novel therapeutic approach for CHOM. These findings open new avenues for developing Prmt1 inhibitors as CHOM treatments.

Supplementary Information

The online version contains supplementary material available at <https://doi.org/10.1186/s13062-025-00652-9>.

Supplementary Material 1

Supplementary Material 2

Supplementary Material 3

Acknowledgements

The authors thank the staff of the experimental center and animal facility of Honghui Hospital for their contributions to experimental guidelines and animal maintenance.

Author contributions

Xun Chen: Methodology, Software, Data curation, Investigation. Ning Duan: Investigation, Software, Resources. Wentao Zhang: Investigation, Validation. Tao Song: Visualization, Data curation. Fei Cong: Conceptualization, Resources, Writing - original draft, Writing - review & editing.

Funding

Funding information is not available.

Data availability

No datasets were generated or analysed during the current study.

Declarations

Ethics approval and consent to participate

The animal experiments were performed according to a protocol (XAH-22-012) approved by the Animal Care Committee of Honghui Hospital.

Consent for publication

Not applicable.

Competing interests

The authors declare no competing interests.

Author details

¹Department of Orthopaedics, Honghui Hospital, Xi'an Jiaotong University, Xi'an 710054, Shaanxi, China

Received: 4 February 2025 / Accepted: 28 April 2025

Published online: 09 May 2025

References

- Urish KL, Cassat JE. Staphylococcus aureus osteomyelitis: bone, Bugs, and surgery. *Infect Immun*. 2020;88:e00932–19.
- Jha Y, Chaudhary K. Diagnosis and treatment modalities for osteomyelitis. *Cureus*. 2022;14:e30713.
- Ellur V, Kumar G, Sampath JS. Treatment of chronic hematogenous osteomyelitis in children with antibiotic impregnated calcium sulphate. *J Pediatr Orthop*. 2021;41(2):127–31.
- Jones HW, Beckles VL, Akinola B, Stevenson AJ, Harrison WJ. Chronic haematogenous osteomyelitis in children: an unsolved problem. *J Bone Joint Surg Br*. 2011;93(8):1005–10.
- Jin M, Wu X, Hu J, Chen Y, Yang B, Cheng C, Yang M, Zhang X. EGFR-MEK1/2 cascade negatively regulates bactericidal function of bone marrow macrophages in mice with Staphylococcus aureus osteomyelitis. *PLoS Pathog*. 2024;20(8):e1012437.
- Ning R, Zhang X, Guo X, Li Q. Attachment of Staphylococcus aureus is required for activation of nuclear factor kappa B in human osteoblasts. *Acta Biochim Biophys Sin (Shanghai)*. 2010;42(12):883–92.
- Jin T, He P, Yang R, Geng R, Yang G, Xu Y. CHI3L1 promotes Staphylococcus aureus-induced osteomyelitis by activating p38/MAPK and Smad signaling pathways. *Exp Cell Res*. 2021;403(1):112596.
- Ormsby RT, Zelmer AR, Yang D, Gunn NJ, Starczak Y, Kidd SP, Nelson R, Solomon LB, Atkins GJ. Evidence for osteocyte-mediated bone-matrix degradation associated with periprosthetic joint infection (PJI). *Eur Cell Mater*. 2021;42:264–80.
- Rautiainen L, Cirko A, Pavare J, Balmaks R, Grope I, Katirilo I, Gersono G, Trejtkovs P, Gardovska D. Assessment of ADAMTS-13 level in hospitalized children with serious bacterial infections as a possible prognostic marker. *Med (Kaunas)*. 2019;55(8):503.
- Campbell MJ, Bustamante-Gomez C, Fu Q, Beenken KE, Reyes-Pardo H, Smeltzer MS, O'Brien CA. RANKL-mediated osteoclast formation is required for bone loss in a murine model of Staphylococcus aureus osteomyelitis. *Bone*. 2024;187:117181.

11. Varghese S. Matrix metalloproteinases and their inhibitors in bone: an overview of regulation and functions. *Front Biosci.* 2006;11:2949–66.
12. Tang BL. ADAMTS: a novel family of extracellular matrix proteases. *Int J Biochem Cell Biol.* 2001;33(1):33–44.
13. Amirzad H, Dadashpour M, Zarghami N. Application of decellularized bone matrix as a bioscaffold in bone tissue engineering. *J Biol Eng.* 2022;16(1):1.
14. Rifai A, Weerasinghe DK, Tilaye GA, Nisbet D, Hodge JM, Pasco JA, Williams LJ, Samarasinghe RM, Williams RJ. Biofabrication of functional bone tissue: defining tissue-engineered scaffolds from nature. *Front Bioeng Biotechnol.* 2023;11:1185841.
15. Gimza BD, Cassat JE. Mechanisms of antibiotic failure during *Staphylococcus aureus* osteomyelitis. *Front Immunol.* 2021;12:638085.
16. Wu Q, Schapira M, Arrowsmith CH, Barsyte-Lovejoy D. Protein arginine methylation: from enigmatic functions to therapeutic targeting. *Nat Rev Drug Discov.* 2021;20(7):509–30.
17. Guccione E, Richard S. The regulation, functions and clinical relevance of arginine methylation. *Nat Rev Mol Cell Biol.* 2019;20(10):642–57.
18. Liu LM, Tang Q, Hu X, Zhao JJ, Zhang Y, Ying GG, Zhang F. Arginine methyltransferase PRMT1 regulates p53 activity in breast Cancer. *Life (Basel).* 2021;11(8):789.
19. Bayen S, Saini S, Gaur P, Duraisamy AJ, Kumar Sharma A, Pal K, Vats P, Singh SB. PRMT1 promotes hyperglycemia in a FoxO1-dependent manner, affecting glucose metabolism, during hypobaric hypoxia exposure, in rat model. *Endocrine.* 2018;59(1):151–63.
20. Martinez S, Sentsis S, Poulard C, Trédan O, Le Romancer M. Role of PRMT1 and PRMT5 in breast Cancer. *Int J Mol Sci.* 2024;25(16):8854.
21. Lai Y, Li X, Li T, Li X, Nyunoya T, Chen K, Kitsios G, Nourai M, Zhang Y, McVerry BJ, Lee JS, Mallapalli RK, Zou C. Protein arginine N-methyltransferase 4 (PRMT4) contributes to lymphopenia in experimental sepsis. *Thorax.* 2023;78(4):383–93.
22. Haghbandish N, Baldwin RM, Moretton A, Dawit HT, Adhikary H, Masson JY, Mazroui R, Trinkle-Mulcahy L, Côté J. PRMT7 methylates eukaryotic translation initiation factor 2a and regulates its role in stress granule formation. *Mol Biol Cell.* 2019;30(6):778–93.
23. Liu H, Lyu H, Jiang G, Chen D, Ruan S, Liu S, et al. ALKBH5-Mediated m6A demethylation of GLUT4 mRNA promotes Glycolysis and resistance to HER2-Targeted therapy in breast Cancer. *Cancer Res.* 2022;82:3974–86.
24. Bellelli R, Castellone MD, Guida T, Limongello R, Dathan NA, Merolla F, Cirafici AM, Affuso A, Masai H, Costanzo V, Grieco D, Fusco A, Santoro M, Carlomagno F. NCOA4 transcriptional coactivator inhibits activation of DNA replication origins. *Mol Cell.* 2014;55(1):123–37.
25. Bannister AJ, Kouzarides T. The CBP co-activator is a histone acetyltransferase. *Nature.* 1996;384(6610):641–3.
26. Yang M, Zhang Y, Liu G, Zhao Z, Li J, Yang L, Liu K, Hu W, Lou Y, Jiang J, Liu Q, Zhao P. TIPE1 inhibits osteosarcoma tumorigenesis and progression by regulating PRMT1 mediated STAT3 arginine methylation. *Cell Death Dis.* 2022;13(9):815.
27. Moll UM, Petrenko O. The MDM2-p53 interaction. *Mol Cancer Res.* 2003;1(14):1001–8.
28. Shen J, Li P, Shao X, Yang Y, Liu X, Feng M, Yu Q, Hu R, Wang Z. The E3 ligase RING1 targets p53 for degradation and promotes Cancer cell proliferation and survival. *Cancer Res.* 2018;78(2):359–71.
29. Allton K, Jain AK, Herz HM, Tsai WW, Jung SY, Qin J, Bergmann A, Johnson RL, Barton MC. Trim24 targets endogenous p53 for degradation. *Proc Natl Acad Sci U S A.* 2009;106(28):11612–6.
30. Winston JT, Strack P, Beer-Romero P, Chu CY, Elledge SJ, Harper JW. The SCF-beta-TRCP-ubiquitin ligase complex associates specifically with phosphorylated destruction motifs in I-kappaBalpha and beta-catenin and stimulates I-kappaBalpha ubiquitination in vitro. *Genes Dev.* 1999;13(3):270–83.
31. Lee DF, Kuo HP, Liu M, Chou CK, Xia W, Du Y, Shen J, Chen CT, Huo L, Hsu MC, Li CW, Ding Q, Liao TL, Lai CC, Lin AC, Chang YH, Tsai SF, Li LY, Hung MC. KEAP1 E3 ligase-mediated downregulation of NF-kappaB signaling by targeting IKKbeta. *Mol Cell.* 2009;36(1):131–40.
32. Zhang L, Tran NT, Su H, Wang R, Lu Y, Tang H, Aoyagi S, Guo A, Khodadadi-Jamayran A, Zhou D, Qian K, Hricik T, Côté J, Han X, Zhou W, Laha S, Abdel-Wahab O, Levine RL, Raffel G, Liu Y, Chen D, Li H, Townes T, Wang H, Deng H, Zheng YG, Leslie C, Luo M, Zhao X. Cross-talk between PRMT1-mediated methylation and ubiquitylation on RBM15 controls RNA splicing. *Elife.* 2015;4:e07938.
33. Sanchez-Bailon MP, Choi SY, Dufficy ER, Sharma K, McNeer GS, Gunnell E, Chiang K, Sahay D, Maslen S, Stewart GS, Skehel JM, Dreveny I, Davies CC. Arginine methylation and ubiquitylation crosstalk controls DNA end-resection and homologous recombination repair. *Nat Commun.* 2021;12(1):6313.
34. Calabretta S, Vogel G, Yu Z, Choquet K, Darbelli L, Nicholson TB, Kleinman CL, Richard S. Loss of PRMT5 promotes PDGFRa degradation during oligodendrocyte differentiation and myelination. *Dev Cell.* 2018;46(4):426–e4405.
35. Liu CJ. The role of ADAMTS-7 and ADAMTS-12 in the pathogenesis of arthritis. *Nat Clin Pract Rheumatol.* 2009;5(1):38–45.
36. Wang WJ, Yu XH, Wang C, Yang W, He WS, Zhang SJ, Yan YG, Zhang J. MMPs and ADAMTSs in intervertebral disc degeneration. *Clin Chim Acta.* 2015;448:238–46.
37. Konda M, Kitabatake M, Ouji-Sageshima N, Tomomura R, Furukawa R, Sonobe S, Terada-Ikeda C, Takeda M, Kawaguchi M, Ito T. A disintegrin and metalloproteinase with thrombospondin motifs 4 regulates pulmonary vascular hyperpermeability through destruction of glycocalyx in acute respiratory distress syndrome. *Int J Mol Sci.* 2023;24(22):16230.
38. Santamaria S, de Groot R. ADAMTS proteases in cardiovascular physiology and disease. *Open Biol.* 2020;10(12):200333.
39. Kumar S, Rao N, Ge R. Emerging roles of ADAMTSs in angiogenesis and Cancer. *Cancers (Basel).* 2012;4(4):1252–99.
40. Wassif RK, Elkayal M, Shamma RN, Elkhesheh SA. Recent advances in the local antibiotics delivery systems for management of osteomyelitis. *Drug Deliv.* 2021;28:2392–414.

Publisher's note

Springer Nature remains neutral with regard to jurisdictional claims in published maps and institutional affiliations.